AD-A128 004 WALL LAYER STRUCTURE AND DRAG REDUCTION: BURSTING RATES (U) PURDUE UNIV LAFAYETTE IN SCHOOL OF MECHANICAL ENGINEERING W G TIEDERMAN ET AL. DEC 82 PME-FM-82-2 1/1

UNCLASSIFIED N00014-81-C-0210 F/G 20/4 NL

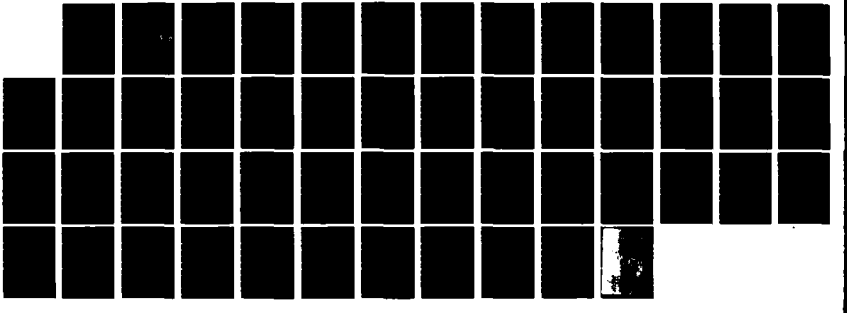

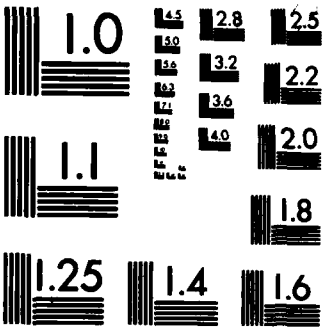

(13)

Report PME-FM-82-2

AD-A128004

WALL LAYER STRUCTURE AND DRAG REDUCTION

Bursting rates

William G. Tiederman and Thomas S. Luchik
School of Mechanical Engineering
Purdue University
West Lafayette, Indiana 47907

December 1982

Technical Report for Period 02 January 1982 - 31 December 1982

Approved for public release; distribution unlimited

Prepared for

DAVID W. TAYLOR NAVAL SHIP RESEARCH AND DEVELOPMENT CENTER
Bethesda, MD 20084

OFFICE OF NAVAL RESEARCH
800 N. Quincey St.
Arlington, VA 22217

SECURITY CLASSIFICATION OF THIS PAGE (When Data Entered)

REPORT DOCUMENTATION PAGE	READ INSTRUCTIONS BEFORE COMPLETING FORM
1. REPORT NUMBER: PME-FM-82-2 ✓	2. GOVT ACCESSION NO.: AD-A128004
3. RECIPIENT'S CATALOG NUMBER	
4. TITLE (and Subtitle): WALL LAYER STRUCTURE AND DRAG REDUCTION; Bursting rates	5. TYPE OF REPORT & PERIOD COVERED: TECHNICAL REPORT Jan.2,1982 through Dec.31,1982
	6. PERFORMING ORG. REPORT NUMBER
7. AUTHOR(s): William G. Tiederman and Thomas S. Luchik	8. CONTRACT OR GRANT NUMBER(s): N00014-81-0210
9. PERFORMING ORGANIZATION NAME AND ADDRESS: School of Mechanical Engineering, Purdue University, West Lafayette, Indiana 47907	10. PROGRAM ELEMENT, PROJECT, TASK AREA & WORK UNIT NUMBERS: SR0230101, 61153N R02301
11. CONTROLLING OFFICE NAME AND ADDRESS: David W. Taylor Naval Ship Research and Development Center, Code 1505 Bethesda, MD 20084	12. REPORT DATE: December 1982
	13. NUMBER OF PAGES: 46
14. MONITORING AGENCY NAME & ADDRESS(if different from Controlling Office): Office of Naval Research, 800 N. Quincey St., Arlington, VA 22217	15. SECURITY CLASS. (of this report)
	15a. DECLASSIFICATION/DOWNGRADING SCHEDULE

16. DISTRIBUTION STATEMENT (of this Report)

APPROVED FOR PUBLIC RELEASE: DISTRIBUTION UNLIMITED

17. DISTRIBUTION STATEMENT (of the abstract entered in Block 20, if different from Report)

18. SUPPLEMENTARY NOTES

Sponsored by the Naval Sea Systems Command General Hydromechanics Research (GHR) Program Administered by David W. Taylor Naval Ship Research and Development Center, Bethesda, MD 20084

19. KEY WORDS (Continue on reverse side if necessary and identify by block number)

Drag reduction, Turbulent wall flows

20. ABSTRACT (Continue on reverse side if necessary and identify by block number)

The basic objective of this experimental study was to determine how the presence of a drag-reducing polymer solution in various portions of the wall region effects the bursting rate of the coherent wall layer structure and the wall shear stress. This was accomplished by injecting drag-reducing polymer solutions, glycerin solutions (whose viscosity matched those of the polymer solutions) and water into the viscous sublayer of fully developed, two-dimensional channel flows of water. Two injection flow rates and two set of slots

DD FORM 1 JAN 73 1473 EDITION OF 1 NOV 65 IS OBSOLETE
S/N 0102-014-6601 |

SECURITY CLASSIFICATION OF THIS PAGE (When Data Entered)

were used. With thin slots and injection flow rates of 1/10 the sublayer flow rate, results were obtained when the injected solutions were confined almost entirely within the sublayer. With larger slots and injection flow rates equal to the sublayer flow rate, results were obtained for situations where the injected fluid had mixed into the buffer region of the channel flow. Bursting rates were deduced from flow visualization of dyed fluid while wall pressure measurements were used to determine the wall shear stress.

When the drag-reducing solutions are confined to the viscous sublayer, there is no drag reduction and both the spanwise spacing and bursting of the wall layer structure are the same as those for a water flow. Drag reduction begins downstream of the location where the injected fluid begins to mix in significant quantities with the buffer region ($10 < y^+ < 100$) of the channel flow. However, in locations where drag reduction occurs and where the injected fluid is not yet uniformly mixed with the channel flow, the dimensionless spanwise spacing increases and the average time between bursts increases. The wall layer structure appears to be like that of a homogeneous, uniformly mixed, drag-reducing solution. Thus, the additives have a direct effect on the flow processes in the buffer region and the viscous sublayer appears to have a passive role in the interaction of the inner and outer portions of a turbulent wall layer.

TABLE OF CONTENTS

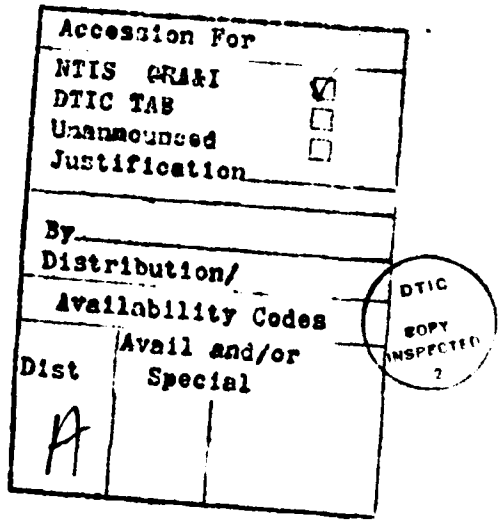

INTRODUCTION

A major difficulty in designing practical, full-scale, systems for controlling turbulence and thereby reducing viscous drag is that the turbulent flow processes are not understood well enough to be modelled accurately. This condition has not prevented engineers from using soluble long-chain polymer molecules for drag reduction in liquid flows. However, it has prevented the development of reliable methods for scaling up laboratory results and for accurately assessing, without large amounts of testing, other potential schemes for drag reduction such as compliant walls. The basic purpose of this experimental study was to gain new knowledge about the physics of turbulent wall flows with and without the addition of drag-reducing polymer solution.

Particular attention was directed toward the coherent structures and cyclic process in the wall region that are responsible for turbulent transport. In part this was due to the fact that significant reductions in the wall shear stress can occur when low concentrations of soluble long-chain polymer molecules are in the near-wall region of turbulent flows [1,2,3]. The critical portion of the wall region where the polymer molecules must be in order to effect the spanwise spacing of the coherent structures is outside the linear portion of the viscous sublayer [4]. It is in this same region where the production and dissipation of turbulent kinetic energy peaks and where the ejection or bursting phase of the turbulent wall structure originates [5,6]. The primary objective of this phase of the experimetnal study was to determine how the average bursting rate of the coherent structures are effected by the presence of drag-reducing polymer solutions in various portions of the wall region.

Experiments were conducted in which two different portions of the wall region contained drag-reducing solution. In both cases, solutions were injected into the viscous sublayer of a fully developed channel flow of water. The slots spanned most of the width in the two 25 cm walls of the 2.5 x 25 cm rectangular cross section channel. In the first case, the bursting measurements were made by marking the injected fluid at the injection slot and by keeping the injection flow rate equal to one-tenth the flow rate in the linear sublayer. Consequently the detected bursts represent the original transport between the sublayer containing the injected

solution and the mainstream water flow.

In the second case two sets of slots were used. Solutions were injected at a rate equal to the flow rate in the linear sublayer through the upstream slot while the downstream slots were used to mark sublayer fluid. In this way bursts were detected in a region where the drag reduction from the upstream slot was near a maximum and the injected solution had mixed with at least a good portion of the original water flow. In both cases the amount of drag reduction was deduced from wall pressure measurements that spanned a region from upstream of the injection slots to the downstream end of the channel.

These experiments differed in one other fundamental way from previous experiments designed to determine bursting rates in homogeneous flows of drag-reducing solutions. The first two experiments that yielded bursting data for drag-reducing flows [7,8] were based on flow visualization methods introduced by Kline et al. [5]. In this method, the procedure is to count all bursts marked by fluid seeped into the wall region from a short spanwise slot. In order to see all of the bursts a rather long field of view is required. For example, in a water flow the bursts will originate from streamwise locations downstream of the slot that typically vary from $100 \leq x^+ \leq 1500$. This is because the marked fluid must be swept into a streak and the streak must lift or migrate away from the wall before it will burst or eject marked wall region fluid into the outer portion of the flow. Similarly at a downstream location where the dyed fluid is exhausted, no new bursts can be detected even though burst are occurring. In both of these earlier studies the streamwise field of view was on the order of $x^+ = 1000$ to 2000. This was an adequate field of view for the water cases. However, as shown by Tiederman et al. [9] this streamwise view probably was not sufficient for the drag-reducing flows where the sublayer streaks are much longer.

Consequently a second method for determining the average time between bursts from dye-slot flow visualization was introduced in Reference 9. This new method was based on the concept that the bursting rate must be constant in a fully developed flow. Hence, if there is a streamwise region where the dyed fluid marks all of the bursts originating from that region, that region will be defined by the extent of the maximum in a plot showing the

number of bursts per unit time as a function of distance from the dye slot. The plausibility of this method was demonstrated in Reference 9 and later developed and proven by one to one comparisons between dye marked bursts and those marked by a vertical hydrogen bubble wire [10]. This new technique is believed to be more reliable and it was used for all the results in this report.

In addition to the data taken with polymer injection, experiments were conducted to determine the effect of Reynolds number on the bursting rate in fully developed water flows. The objective of these experiments was to test methods used to correlate the average time between bursts.

After describing details of the test section, injected fluids and experimental procedures in the next section, the results are presented and analyzed in the third section of this report. The conclusions and recommendations are presented at the end of the report.

EXPERIMENTAL APPARATUS AND PROCEDURES

Apparatus

The experiments were conducted in the flow loop shown in Figure 1. Except for modifications to the test section that will be described later, this is the same flow loop used in the first phase of this study [4]. The essential features include the orifice meter used to determine the recirculating water flow rate and a combination of perforated plates, screen-sponge-screen section, smooth contractions and flow straighteners to yield a smooth flow at the inlet of the two-dimensional channel.

The internal dimensions of the test section's rectangular cross section are 2.5 x 25 cm or 0.980 x 9.84 inches which gives the channel an aspect ratio of 10 to 1. The injection slots are located more than 60 channel widths downstream of the entrance and more than 30 channel widths upstream of the exit. Consequently the flow in the region of the injection slots is typical of fully developed, two-dimensional channel flow.

The injected fluid flows by gravity from reservoirs above the channel, through Gilmont rotameter flow meters and flow control valves to the injection slots. Figure 1 shows how injection fluid was supplied to the modified test section that had four injection slots (two in each wall). Clear fluid from a single large reservoir was piped through two independently controlled flowmeters to the two upstream slots. Separate reservoirs supplied the downstream slots so that clear fluid could be piped to the slot in the top wall while dyed fluid used for flow visualization could be piped to the bottom slot.

The bottom plate for the original test section is shown in Figure 2. each slot was 0.005 inches wide, 8.84 inches long and centered in the 10.84 inch section that formed the 25 cm walls of the test section. As a result fluid was not injected into either the corners or along the 2.5 cm side walls of the channel. These thin slots are perpendicular to the streamwise direction and are therefore referred to as normal slots.

Also shown in Figure 2 are the streamwise locations of the pressure taps that were centered in the bottom wall of the channel. Tap number 1 is 8 inches upstream of the injection slots and tap number 8 is 31 inches downstream of the slots. Of course the most critical taps are those which

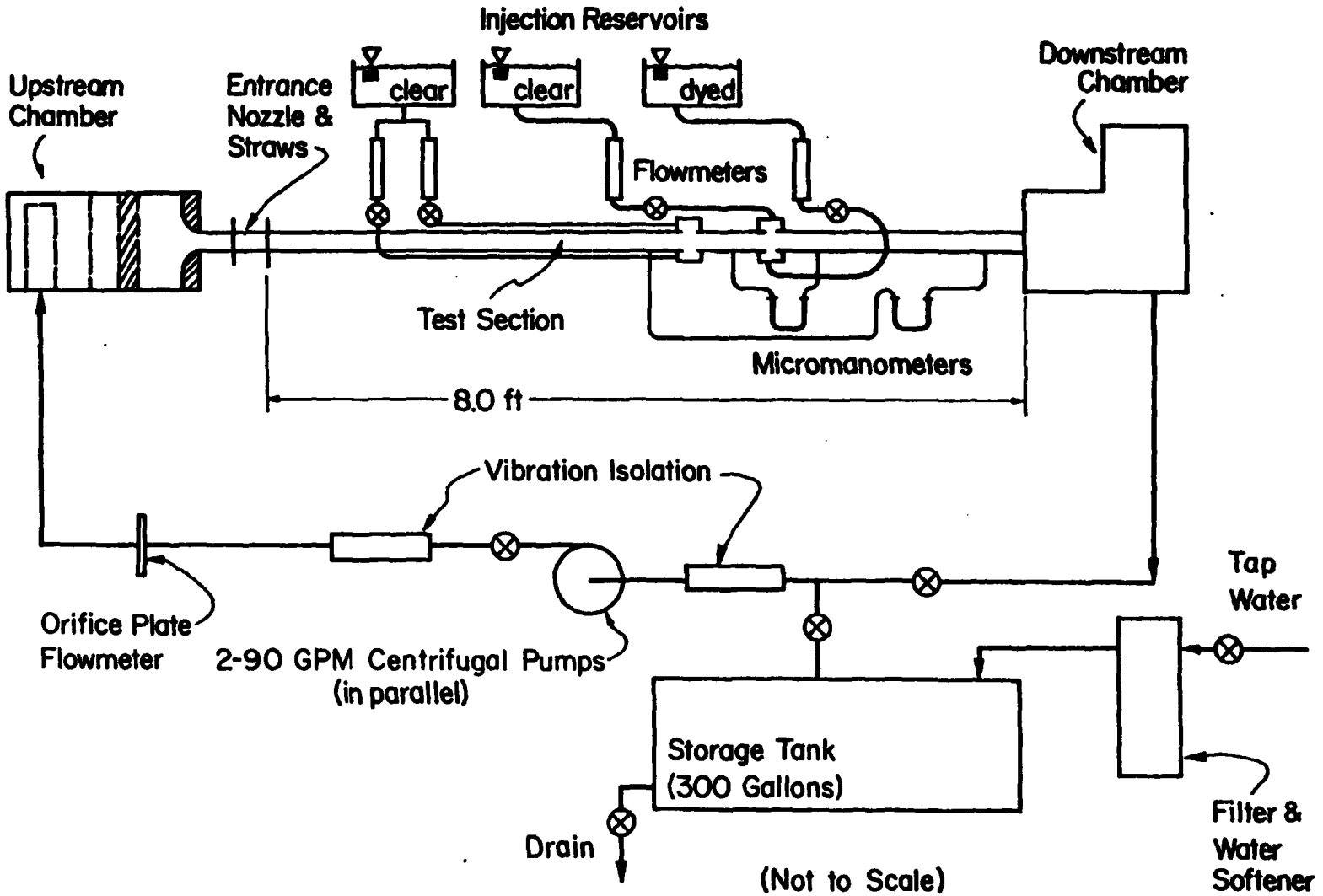

Figure 1. Schematic of flow loop

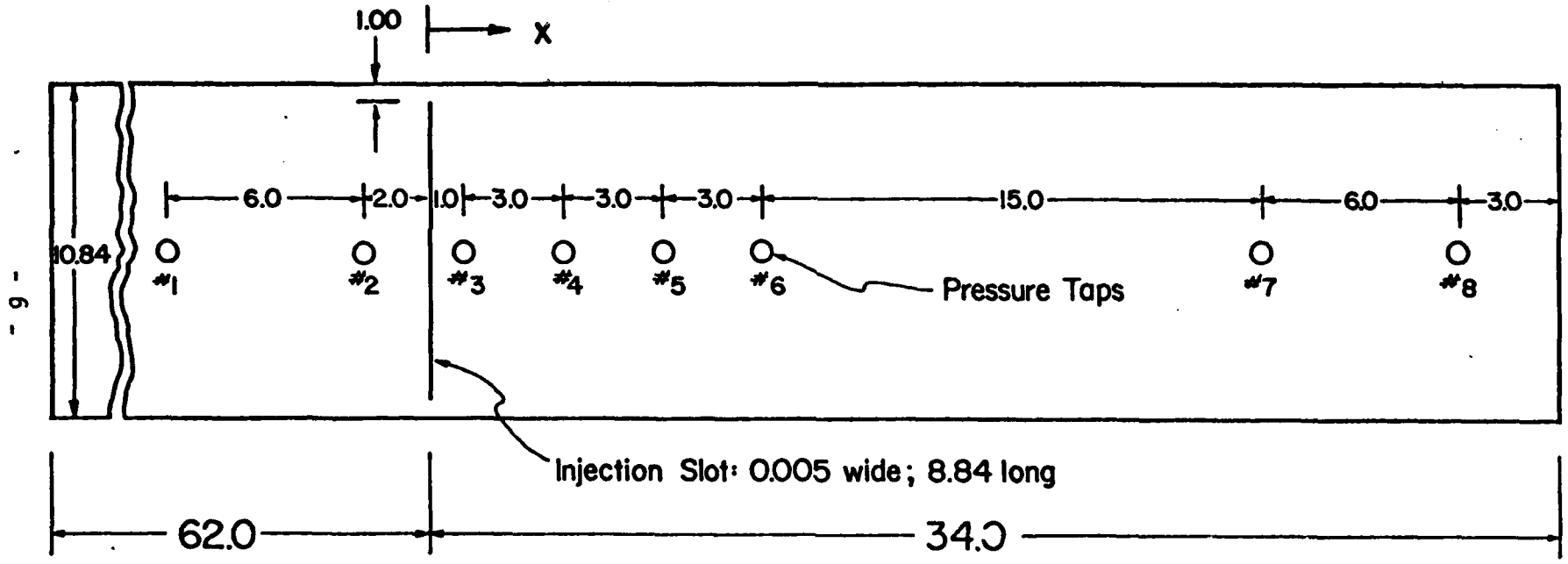

Figure 2. Schematic of bottom wall for the original test section.

are nearest the injection. Each static pressure hole has a diameter of 1/16 inch and a length of 1/8 inch which connects the tap to a 1/4-inch tube glued into the outside of the plastic wall. All holes were drilled carefully to ensure that they are perpendicular with the surface and free of burrs and chips.

The bottom plate of the modified test section is shown in Figure 3. The major addition is Injection Slot 1 which is an inclined, 0.050 inch wide slot. Injection slot 2 is the original, normal slot in this wall and it was used for flow visualization purposes while the larger upstream slot was used for introducing the injected solutions. As before the pressure tap locations are shown in the figure. Note that the distribution of these taps around the slots is slightly different than the configuration for the original bottom plate.

In both test sections the top plate had identical injection slots at the same location as in the bottom plate. However there were no pressure taps in the top plates. Please note that in both Figures 2 and 3 the flow direction is from left to right.

A cross sectional view of the inclined slots is shown in Figure 4. Here the flow direction is from right to left so that the injected fluid enters the channel at an angle of 20° with respect to the flow direction. Also shown in the figure are details of the two pressure taps located just upstream and downstream of the slot in the bottom wall.

Two Gilmont micrometer manometers with carbontetrachloride as the manometer fluid were used to measure the pressure drop. With this manometer fluid which has a specific gravity of 1.591, the pressure measurements could be made with a sensitivity of 1.5×10^{-2} mm or 6×10^{-4} inches of water.

The lighting and camera configuration used to obtain motion pictures of bursts from the sublayer streaks is shown in Figure 5. The camera and strobe light are components of a Video Logic Corporation INSTAR IV high-speed motion analyzer system. The strobe gives the camera an effective exposure time of 10 microseconds while the camera produces 120 pictures per second that are recorded on one-inch video tape. The spanwise thickness of the light plane was adjustable. The typical value was 0.2 inches.

In order to reduce the bursting data the spanwise spacing of the sub-layer streaks must be known. For the 0.005 inch slot experiments, these

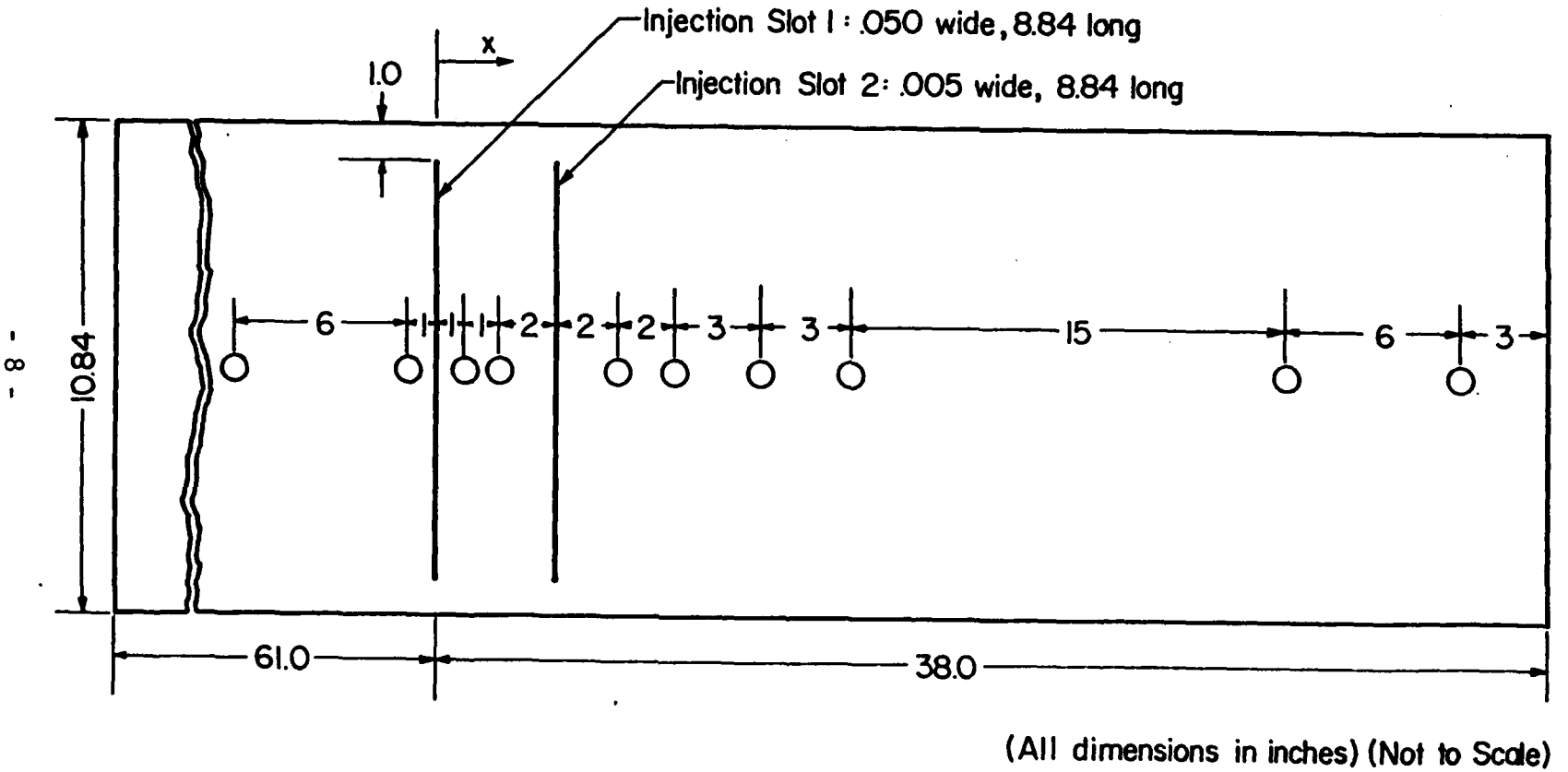

Figure 3. Schematic of bottom wall for the modified test section

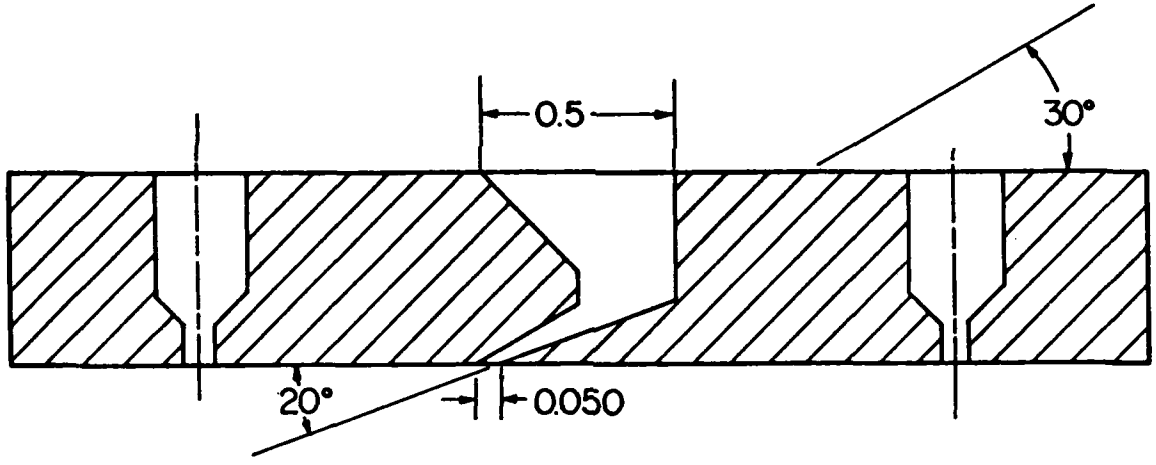

Figure 4. Details of the inclined injection slots, flow is from right to left along the bottom surface of the plate.

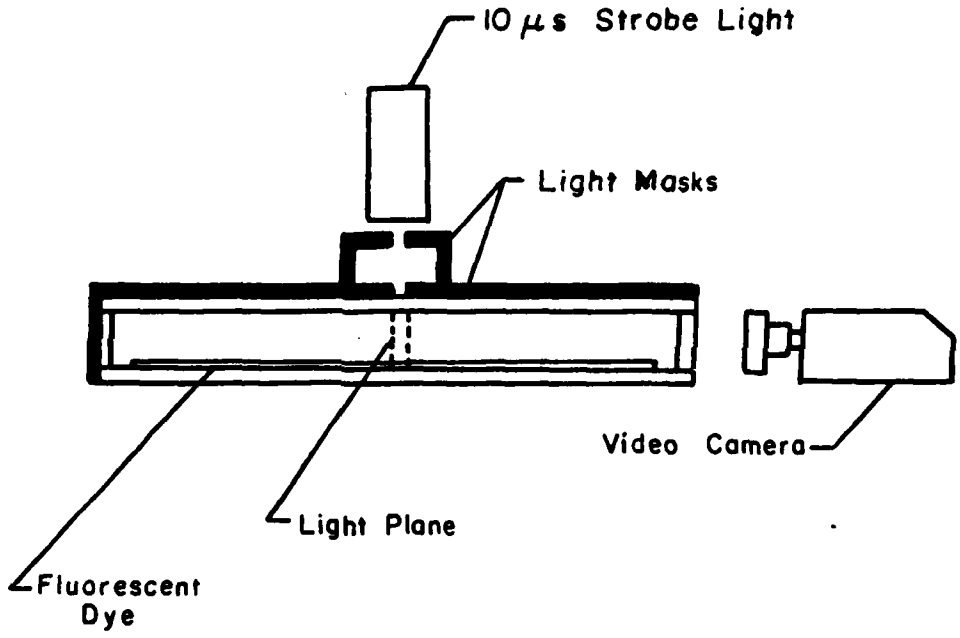

Figure 5. Lighting and camera arrangement for the bursting measurements.

spacing were known [4]. However for the 0.050 inclined slot experiments, these data had to be acquired. This was done using the lighting and camera arrangements described earlier [4] and the techniques discussed by Oldaker and Tiederman [11].

The fluorescent fluid was a 2 gram per liter concentration of Fluorescein disodium salt. The fluids injected into the water flows were water, a 100 ppm solution of SEPARAN AP-273, a 400 ppm solution of AP-273, and two mixtures of glycerin and water that matched the viscosity of the two polymer solutions. Viscosities of all injected fluids, both clear and dyed, were measured with LVT-SCP Wells-Brookfield, 1.565° cone and plate, micro viscometer at shear rates of 115 and 230 sec^{-1}.

The drag reducing capability of the polymer solutions were measured in a separate, horizontal 5/8-inch O.D. (0.553 inch I.D.) tube. The tube was gravity fed from an upstream reservoir while the flow rate was controlled by a valve at the tube's outlet. The flow rate was measured by timing the collection of a fixed mass of fluid while the pressure drop from two taps separated by 78 3/4 inches was measured with an inverted U-tube, water manometer. The upstream pressure tap was 20 inches from the entrance of the tube and the downstream tap was 10 inches upstream of the exit.

Procedures

One of the initial tasks of each experiment was preparation of the micromanometers. [4] When a manometer was sufficiently clean, it would yield accurate results for several days. When not property cleaned, the meniscus between the water and carbontetrachloride would stick to the glass and/or become contaminated and the resulting measurements would be neither reproducible nor accurate. Using deionized water above the carbontetrachloride contributed significantly to the duration of a noncontaminated and stable interface.

Tap water for the main channel flow passed through a filter and a Calgon water softener prior to entering the storage tank for the flow loop. It was de-aerated by heating to about 105°F and then cooled to room temperature before being circulated in the flow loop.

The polymer solutions and glycerin mixtures were made with filtered tap water. The water used for the polymer solutions was boiled and then cooled prior to adding the polymer. These polymer solutions initially were mixed

to produce concentrations of 800 and 2560 ppm. These concentrated mixtures were allowed to hydrate for 12 to 24 hours prior to dilution to 100 and 400 ppm respectively. The quantity of polymer solution prepared in each batch was sufficient to conduct both the drag reduction tests in the 5/8-inch tube and the channel injection experiments.

The basic plan for each experiment was to measure the pressure drop between various taps both with and without injection and to make a video tape of the flow visualization. All of this was done at a constant channel flow rate of 64 GPM. At this flow, the Reynolds number based upon the mass average velocity, hydraulic diamter and viscosity of water at 74°F was 31,600, the shear velocity was 0.0368 m/s (0.12 ft/sec) and the shear rate at the wall with water as the fluid was 1450 sec^{-1}.

Since the viscosity of dilute polymer solutions varies with shear rate, determination of the viscosities of injected polymer solutions required estimates of the shear rate in the wall region. By assuming that the wall shear stress, τ_w, was approximately the same as the water value and that the viscosity, μ, was approximately equal to the value measured at 230 sec^{-1}, the shear rate at the wall, dU/dy was estimated as:

$$\left.\frac{dU}{dy}\right|_o = \frac{\tau_w}{\mu} \qquad (1)$$

The viscosities of the polymer solutions were measured with a viscometer at shear rates of 115 and 230 sec^{-1}. Since the estimated shear rates in the wall region were greater than 230 sec^{-1}, an extrapolation of the measured viscosities was calculated based on the following relationship that experimentally was demonstrated by Oldaker [12]

$$\log_{10}(\mu) = A - B \log_{10}\left(\frac{dU}{dy}\right) \qquad (2)$$

Here A and B are constants. As will be seen later, the conclusions are not effected by these approximations.

REDUCTION AND ANALYSIS OF RESULTS

Experimental Conditions

The experimental conditions summarized in Table 1 are similar to those studied by Tiederman and Bogard [4]. The injection flow rates of each of the fluids tested were 40 ml/min and 400 ml/min which corresponds to 1/10 and 1 times the flow rate in the viscous sublayer respectively. The smaller injection rates were used with the 0.005 inch wide, normal slots while the 0.050 inch wide, inclined slots were used for the higher injection rates. With these combinations of injection rates and slots, the fluids flow into the channel along the walls and do not "jet out" into the main flow.

TABLE 1. Experimental Conditions

Experiment number	Injected fluid	Channel flow rate (GPM)	Injection flow rate (mℓ/min)	Kinematic viscosity of water $\nu \times 10^6$ (m^2/s)	Kinematic viscosity of injection $\nu \times 10^6$ (m^2/s)
006	Water	64	40	.907	.907
011	16% Glycerin	64	40	.907	1.35
027	AP-273 100 ppm	64	40	.907	1.32
033	36% Glycerin	64	40	.907	2.71
042	AP-273 400 ppm	64	40	.907	2.34
097	AP-273 100 ppm	64	400	.907	1.11
111	16% Glycerin	64	400	.907	1.28
124	Water	64	400	.907	.907

Demonstration of drag reduction in 5/8-inch tube

A portion of each batch of polymer solution injected into the channel was tested in a 5/8-inch tube to confirm the drag-reducing capability of the homogeneous solution. The results of these tests are shown in Figure 6.

In these homogeneous flows, percent drag reduction, DR, was defined by

$$DR = 100((c_f)_w - (c_f)_p)/(c_f)_w \qquad (3)$$

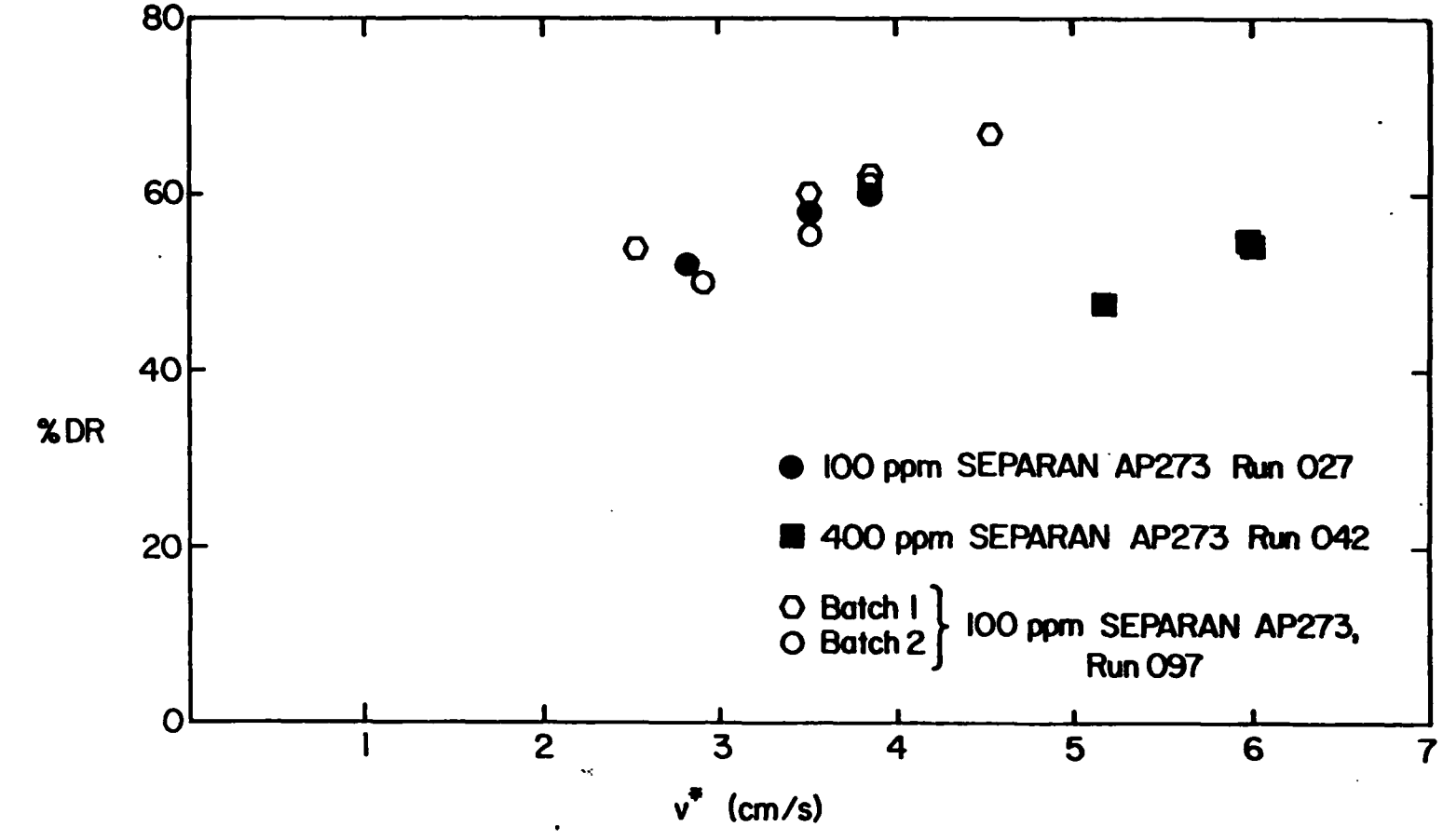

Figure 6. Drag reduction of polymer solutions in 5/8-inch tube.

where $(c_f)_p$ is the skin friction coefficient for the polymer solution and $(c_f)_w$ is the skin friction coefficient for a water flow that has the same flow rate as the polymer solution. The latter is calculated using the correlation for Newtonian fluids

$$c_f = 0.079\ Re^{-1/4} \tag{4}$$

The skin friction coefficient is defined by

$$c_f = \frac{\tau_w}{\frac{1}{2}\rho U^2} \tag{5}$$

and the Reynolds number, Re, is

$$Re = \frac{UD}{\nu} \tag{6}$$

where ρ is the density of the fluids, U is the mass average velocity and D is the internal diameter of the tube. Since the flow in the section between the pressure taps is fully developed, the pressure gradient, $\Delta P/\Delta x$, and wall shear stress are related by

$$\frac{\Delta P}{\Delta x} = \tau_w\ (4/D) \tag{7}$$

Consequently pressure drop measurements are used to calculate the skin friction coefficient for the polymer flows.

As these results clearly show, all polymer solutions injected into the channel were capable of producing drag reduction. Moreover when these results are considered along with those presented in Figure 4 of Reference 4, is is also clear that the polymer solutions are very uniform from batch to batch and that the fluorescent dye did not degrade the polymer solutions.

The 50 to 60 percent drag reduction obtained with the 100 ppm solutions is quite similar to the drag reduction obtained in homogeneous channel flows of this same polymer solution [11]. The value of 60% is close to the maximum value that one could expect to achieve in the present channel. Finally, the 400 ppm results in the tube fall below the 100 ppm results due to the higher viscosity of the more concentrated solution and the relatively small tube diameter.

Two-dimensional nature of injection

As described earlier, the slots were designed so that the polymer solutions would not flow into the corners of the channel. This hypothesized result was checked and confirmed by flow visualizations of ejections marked by dyed fluid from the 0.005 inch slots. The thin light slit technique was used with the slit aligned in the flow direction and placed in the channel at distances from the side wall of 0.25, 0.375, 0.50, and 5.0a where a is the channel height. Recall that the injection slot edge is located 0.5a from the side wall. Ejections were then counted at each spanwise location and compared with the value obtained in the full detection region in the center of the channel, z=5a.

The results are shown in Figure 7. It is clearly shown that near the side wall (0.25a) very few ejections were marked. Thus one can conclude that very little dye was transferred from the slot edge to the side wall region. Close to the slot edge (.375a) still only approximately one half of the ejections seen in the center of the channel were marked. At the slot edge the value for the number of ejections marked in the full detection region reaches 86.4% of the ejections seen in the center of the channel. From these results one can conclude that the flow in the center portion of the channel is two dimensional and that the side walls have little, if any, measurable effect on the flow in the center region.

Method for deducing drag reduction in the channel

The objective of the pressure drop measurements was to determine how the injected fluids effected the viscous drag in the fully developed channel flow. This was done by comparing the wall shear stress when fluid was being injected, $(\tau_w)_i$ to the wall shear stress, τ_w, when there was no injection.

For the fully developed flow when there is no injection

$$\tau_w = \frac{wa}{2(w+a)} \frac{\Delta P}{\Delta x} \tag{8}$$

When injection occurs the situation is more complex because the average shear stress at a given cross section, $\overline{\tau}_w$, is the area weighted value or

$$\overline{\tau}_w = \frac{(\tau_w)_i A_i + \tau_w (A-A_i)}{A} \tag{9}$$

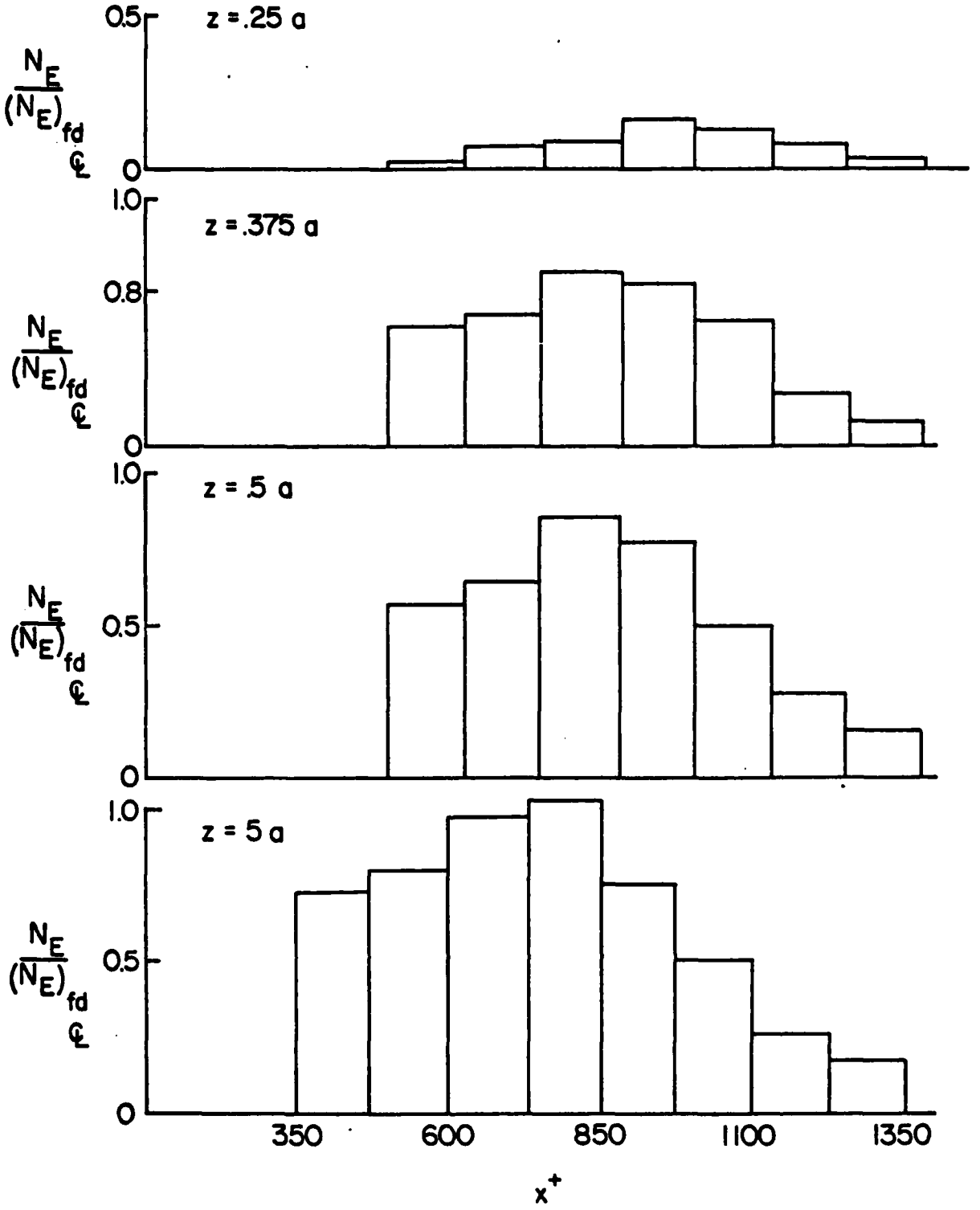

Figure 7. Spanwise variation of ejection histograms showing two-dimensional nature of the injection slots.

Here A_i is the surface area covered by the injected fluid and it is assumed that the shear stress for the surface area not covered by injected fluid is best estimated by the fully developed, no injection value. Neglecting changes in streamwise momentum flux, the average shear stress is given by

$$\bar{\tau}_w = \frac{wa}{2(w+a)} \left(\frac{\Delta P}{\Delta x}\right)_i \tag{10}$$

where $(\Delta P/\Delta x)_i$ is the pressure gradient with injection. Equations 9 and 10 can then be solved for $(\tau_w)_i$ which is then used to calculate the percent drag reduction in the channel according to

$$DR = 100 \left\{ \frac{\tau_w - (\tau_w)_i}{\tau_w} \right\} \tag{11}$$

This procedure is slightly different than the procedure used in Reference 4 and yields about 22% higher values. This increase simply reflects the fact that the polymer solution will not reduce the viscous drag on surfaces that it does not cover. Thus the drag reduction given by Equation 11 yields the two-dimensional value downstream of the slots.

Pressure drop results for the 0.005-inch, normal slots

Injection of the water through the injection slot had no effect on pressure drop when compared to the no injection situation except in the immediate vicinity of the injection slot. At this location a negative drag reduction was measured which corresponds to an increase in pressure drop (Table 2). This is due to the fact that the mainstream flow has to transfer momentum to injected fluid in the main flow direction. Recall that the injection fluid was injected perpendicular to the main flow direction.

Results of the 16% glycerin solution are shown in Table 3. Again the injection of this fluid had little or no effect on the pressure drop measurement except near the injection slot.

TABLE 2. Pressure Drop Results for Water Injection, Run 006

Pressure taps	Distance between taps (inches)	Average streamwise distance (inches)	Manometer deflections No injection h (inches x 10^3)	Injection h_i (inches x 10^3)	Drag reduction (%)
2-3	3.0	-0.5	47	48	-2.6
3-4	3.0	2.5	56	56	0.0
1-8	39.0	11.5	727	733	-1.0

TABLE 3. Pressure Drop Results for 16% Glycerin Injection, Run 011

Pressure taps	Distance between taps (inches)	Average streamwise distance (inches)	Manometer deflections No injection h (inches x 10^3)	Injection h_i (inches x 10^3)	Drag reduction (%)
2-3	3.0	-0.5	44	45	-2.8
4-5	3.0	5.5	63	63	0.0
6-7	15.0	17.5	269	268	0.5
1-8	39.0	11.5	732	732	0.0

As expected the 100 ppm Separan AP-273 yielded appreciable drag reduction. Pressure drop results for this fluid are given in Table 4 and a comparison for the 16% glycerin and the 100 ppm polymer solution is shown in Figure 8. It is clear that no matter what the injection fluid is, there occurs a drag increase in the vicinity of the injection slot, although the increase is much more pronounced in the case of the polymer injection. The onset of positive drag reduction occurs at x=1.6 inches, peaking to a value of 22.4% at x=5.5 inches. It should be noted that this peak value is less than 1/2 the value that would be expected for a homogeneous 100 ppm solution.

In Figure 8 and all subsequent figures of this type, the horizontal line with brackets through each data point show the Δx over which the pressure drop was measured. The curve is then drawn so that the area under the curve is the same as the area under the horizontal lines.

Figure 9 gives a comparison of drag reduction for the 400 ppm polymer solution and the 36% glycerin solution. Again a severe drag increase was seen in the vicinity of the injection slot for the injection of the polymer

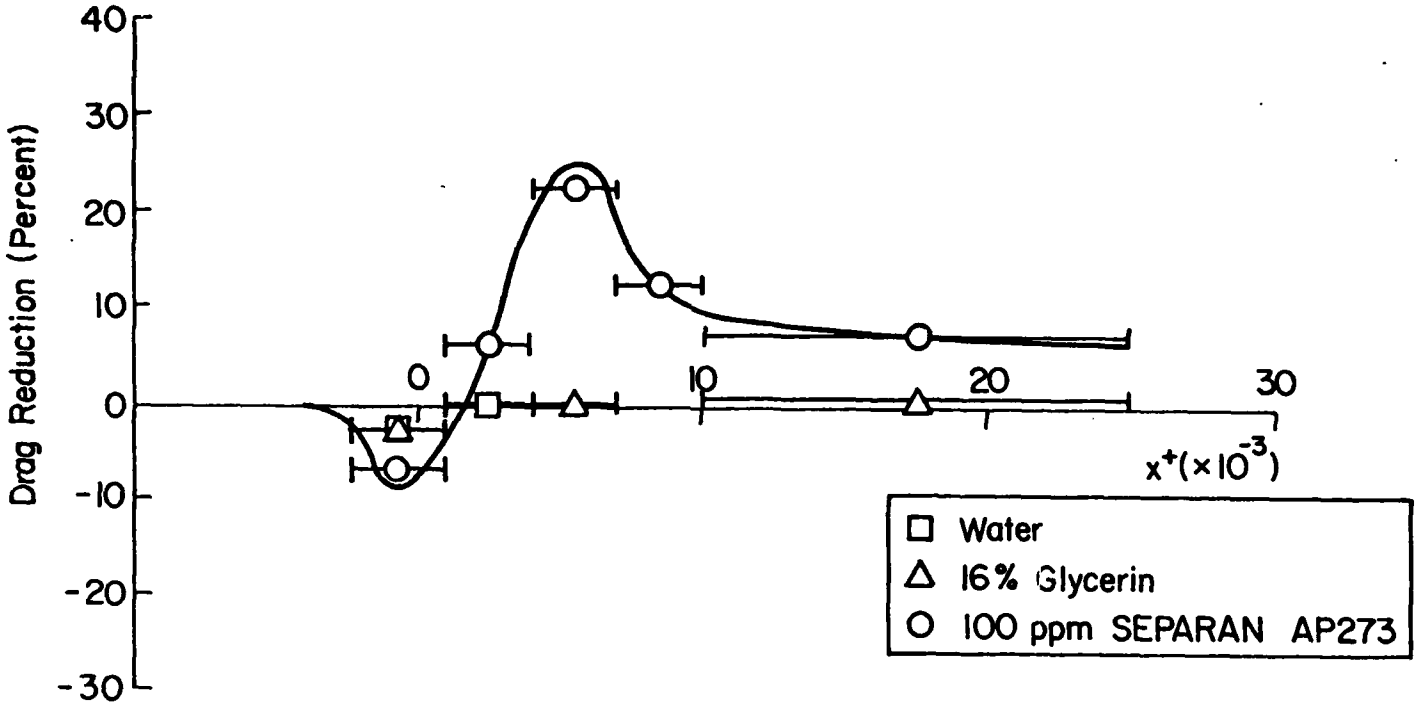

Figure 8. Drag reduction results for the injection of water, 16% glycerin, and 100 ppm solution of AP-273 into the channel flow of water through the 0.005-inch slots.

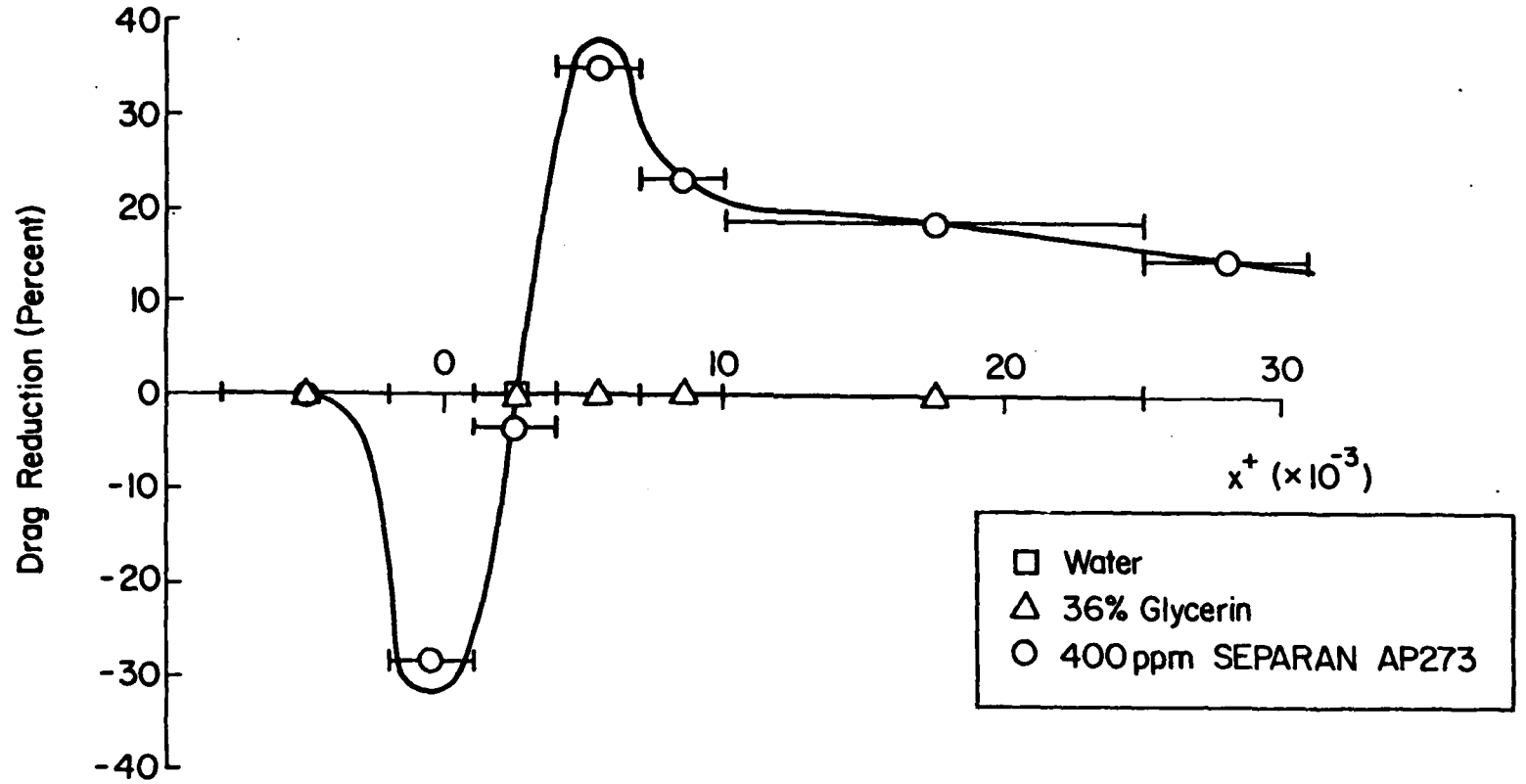

Figure 9. Drag reduction results for the injection of water, 36% glycerin, and 400 ppm solution of AP-273 into the channel flow of water through the 0.005-inch slots.

solution. The onset of positive drag reduction occurred at x=2.6 inches. The peak value of drag reduction again occurred at x=5.5 inches having a value of 35.0 percent. This value is significantly higher than the value found for the 100 ppm polymer solution yet still only about three-fifths the value expected for a homogeneous 400 ppm polymer solution. Tabular results for the 36% glycering solution and 400 ppm polymer solution are given in Tables 5 and 6 respectively.

TABLE 4. Pressure Drop Results for 100 ppm Polymer Injection, Run 027

Pressure taps	Distance between taps (inches)	Average streamwise distance (inches)	Manometer deflections No injection h (inches x 10^3)	Injection h_i (inches x 10^3)	Drag reduction (%)
2-3	3.0	-0.5	36	38	-6.8
3-4	3.0	2.5	61	58	6.0
4-5	3.0	5.5	71	58	22.4
5-6	3.0	8.5	50	45	12.2
6-7	15.0	17.5	272	257	6.7
1-8	39.0	11.5	727	703	4.0

TABLE 5. Pressure Drop Results for 36% Glycerin Injection, Run 033

Pressure taps	Distance between taps (inches)	Average streamwise distance (inches)	Manometer deflections No injection h (inches x 10^3)	Injection h_i (inches x 10^3)	Drag reduction (%)
1-2	6.0	-5.0	111	111	0.0
2-3	3.0	-0.5	78	80	-3.1
3-4	3.0	2.5	74	74	0.0
4-5	3.0	5.5	66	66	0.0
5-6	3.0	8.5	53	53	0.0
6-7	15.0	17.5	272	272	0.0
1-8	39.0	11.5	735	735	0.0

TABLE 6. Pressure Drop Results for 400 ppm Polymer Injection, Run 042

Pressure taps	Distance between taps (inches)	Average streamwise distance (inches)	Manometer deflections No injection h (inches x 10^3)	Injections h_j (inches x 10^3)	Drag reduction (%)
1-2	6.0	-5.0	107	107	0.0
2-3	3.0	-0.5	30	37	-28.6
3-4	3.0	2.5	64	66	-3.8
4-5	3.0	5.5	70	50	35.0
5-6	3.0	8.5	48	39	23.0
6-7	15.0	17.5	244	207	18.6
7-8	6.0	28.0	120	106	14.3
1-8	39.0	11.5	709	637	12.4

The results of these drag reduction experiments show that although both polymer solutions were capable of achieving drag reduction, neither came close to the value expected for the homogeneous solutions. Although the 400 ppm polymer solution showed much greater drag reduction capability in the channel, the severe drag increase in the vicinity of the injection slot tends to make this solution undesirable. On the other hand the 100 ppm polymer solution did not show as much drag reduction in the channel but it also did not show as much drag increase at the injection slot. These results are almost exactly the same as those reported for the streak spacing study [4].

Pressure drop results for the 0.050-inch, inclinded slots

Results for the water injection are given in Table 7. As expected these results show that the water injection has a marginal effect on the pressure field in the channel except in the immediate vicinity of the injection slot. It should be noted that the drag increase in the region is nearly ten times the amount found for the previous water injection case.

Table 8 shows the corresponding results for the 16% glycerin solution. Again there is a negligible effect on the pressure field except in the near slot region, as expected.

TABLE 7. Pressure Drop Results for Water Injection, Run 111

Pressure taps	Distance between taps (inches)	Average streamwise distance (inches)	Manometer deflections No injection h (inches x 10^3)	Injections h_i (inches x 10^3)	Drag reduction (%)
1-2	6.0	-4.0	73.8	75.0	-2.0
2-4	3.0	0.5	66.2	84.0	-32.9
4-6	6.0	5.0	129.4	129.0	0.4
6-7	3.0	9.5	77.0	77.8	-1.3
7-8	3.0	12.5	50.4	51.4	-2.4
8-9	15.0	21.5	296.6	298.0	-0.6
9-10	6.0	32.0	80.7	80.7	0.0
1-10	42.0	14.0	798.0	799.5	-0.2

TABLE 8. Pressure Drop Results for 16% Glycerin Injection, Run 124

Pressure taps	Distance between taps (inches)	Average streamwise distance (inches)	Manometer deflections No injection h (inches x 10^3)	Injections h_i (inches x 10^3)	Drag reduction (%)
1-2	6.0	-4.0	79.0	79.0	0.0
2-4	3.0	0.5	62.3	84.3	-43.22
4-5	4.0	4.0	76.0	80.3	-6.9
4-6	6.0	5.0	124.0	128.8	-4.7
5-6	2.0	7.0	39.8	41.5	-5.2
8-9	15.0	21.5	298.0	298.0	0.0
9-10	6.0	32.0	124.0	124.0	0.0

When the 100 ppm SEPARAN AP-273 polymer solution was introduced through the injection slots, there was a noticeable effect on the pressure field in the channel. The results for all three fluids tested are shown in Figure 10. From the figure it is evident that a maximum drag reduction of approximately 30% is achieved at x=10 inches and maintained for a streamwise distance of 15 inches. One should also note that although the drag reduction is achieved for a desirable distance, the maximum value is still only one half of that expected for the homogeneous 100 ppm polymer solution. The onset of positive drag reduction occurs at x=3 inches nearly twice the value obtained earlier.

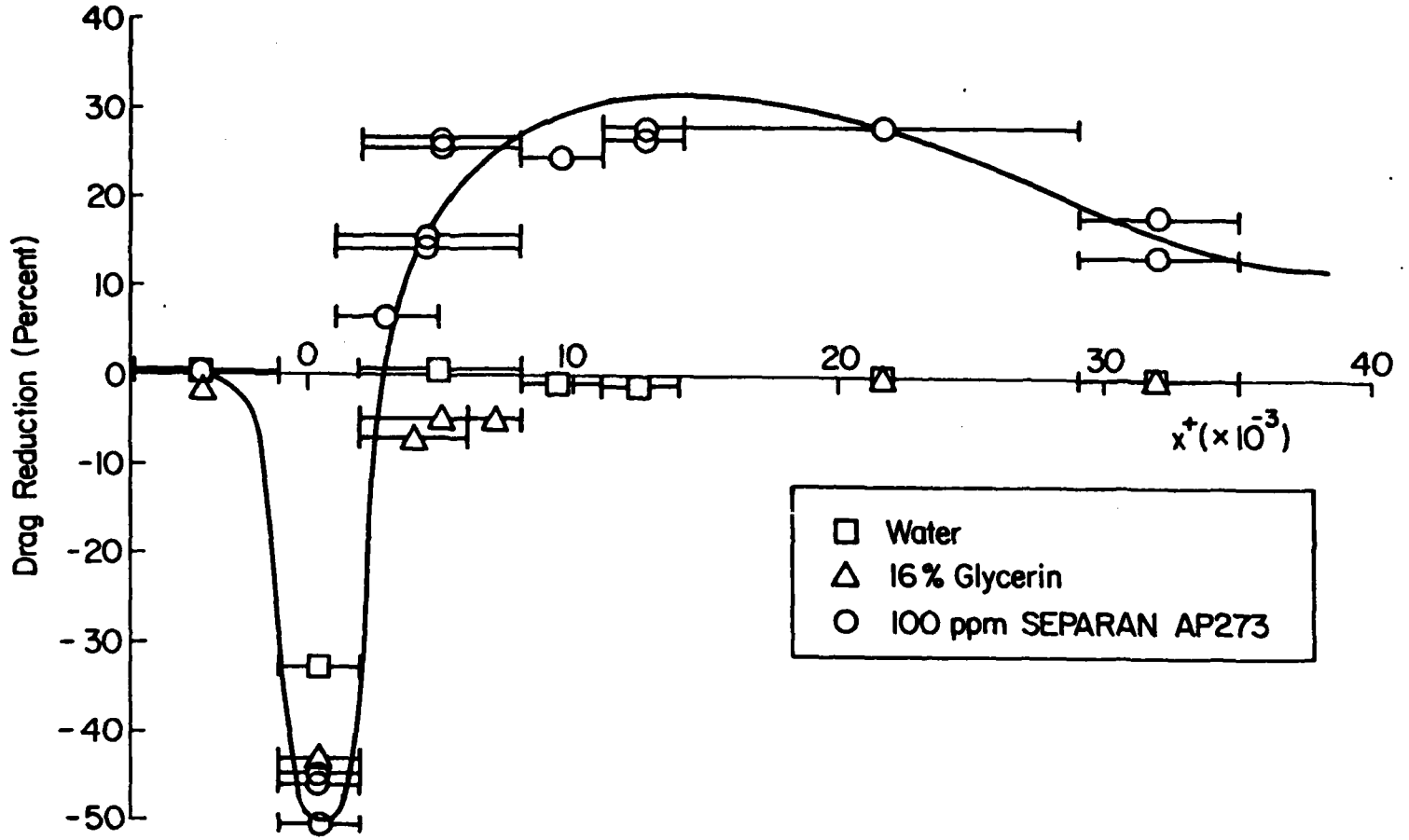

Figure 10. Drag reduction results for the injection of water, 16% glycerin and 100ppm solution of AP-273 into the channel flow of water through 0.050-inch slots.

It is interesting to note that the drag increase in the vicinity of the injection slot (47%) is roughly seven times that of the normal injection case. Tabular results of the 100 ppm case are shown in Table 9.

TABLE 9. Pressure Drop Results for 100 ppm Polymer Injection, Run 097

Pressure taps	Distance between taps (inches)	Average streamwise distance (inches)	Manometer deflections No injection h (inches x 10^3)	Injection h_i (inches x 10^3)	Drag reduction (%)
1-2	6.0	-4.0	99.8	98.8	1.2
2-4	3.0	0.5	76.8	104.6	-44.3
2-4	3.0	0.5	68.0	93.0	-45.0
2-4	3.0	0.5	68.4	96.8	-50.8
3-5	4.0	3.0	77.0	73.0	6.4
3-6	7.0	4.5	168.8	147.8	15.2
3-6	7.0	4.5	153.0	135.0	14.4
4-6	6.0	5.0	118.5	92.8	26.5
4-6	6.0	5.0	124.5	98.5	25.6
6-7	3.0	9.5	84.6	67.6	24.6
7-8	3.0	12.5	53.8	41.6	27.8
7-8	3.0	12.5	43.4	34.0	26.5
8-9	15.0	21.5	271.6	209.8	27.9
9-10	6.0	32.0	109.6	93.4	18.1
9-10	6.0	32.0	97.0	86.2	13.6
1-10	42.0	14.0	802.0	717.2	12.9
1-10	42.0	14.0	817.0	733.7	12.5

Analysis of drag increase near the injection slots

From the flow visualization of the streaks reported earlier [4], it was clear that the injected polymer solutions initially did not mix as well with the mainstream water flow. Two types of one-dimensional calculations were performed to see if this decrease in mixing was sufficient to explain the differences between the measured drag increases for the polymer and water injections.

For the case of water injection it was assumed that the water mixes quickly and completely with the mainstream flow. Thus the pressure changes

due to injection were due solely to the added flow rate. That is, during injection the average flow rate downstream of the injection slots was slightly higher than the no injection flow rate. Bernoulli's equation was used to estimate the change in manometer reading at the first tap downstream of the water injection assuming that the velocity profiles were uniform. A comparison of these calculations with the measured values given in Table 10 shows that this simple analysis predicts well the measured changes for the smaller slot.

TABLE 10. Comparison of Measured and Calculated Manometer Deflections for Water Injection (well mixed assumption)

Injection slot	Calculated value of $h-h_i$ (inches x 10^{+3})	Measured value of $h-h_i$ (inches x 10^{+3})
0.005-inch	-0.9	-1.0
0.050-inch	-9.4	-17.8

For the cases where polymer was injected into the channel, it was assumed that there was no mixing between the injected fluid and the fluid in the channel. Consequently the mainstream water flow had a smaller cross-sectional area for flow due to the blockage of the injected fluid. The blockage thickness, δ_i, on each wall was calculated from continuity considerations and from the assumption that the injected fluid flowed along the wall with the linear velocity profile, $U^+ = y^+$. Thus

$$\delta_i = (2\nu Q_i/(d\, v^{*2}))^{1/2} \qquad (12)$$

Here ν is the kinematic viscosity of the injected fluid, d is the length of the injection slot, Q_i is the volumetric flow rate of injected fluid and v^* is the shear velocity. A reasonable estimate of v^* is given by the no injection value. The effect of this effective decrease of flow area on the pressure was then estimated using Bernoulli's equation. A comparison of the calculated and measured difference in the manometer deflections for taps that span the injection slots is shown in Table 11.

The comparisons in Tables 10 and 11 demonstrate that the differences

TABLE 11. Comparison of Calculated and Measured Manometer Deflections for Polymer Injection (unmixed assumption)

Fluid	Injection	Kinematic viscosity of injection ($m^2/s \times 10^{+6}$)	δ_i (mm)	Calculated value of $h-h_i$ (inches $\times 10^{+3}$)	Measured value of $h-h_i$ (inches $\times 10^{+3}$)
water	0.005	0.907	0.063	-13	-1
100 ppm	0.005	1.32	0.076	-16	-2
400 ppm	0.005	2.34	0.101	-21	-7
water	0.050	0.907	0.199	-42	-17.8
100 ppm	0.050	1.11	0.220	-46	-27

in mixing is sufficient to explain the drag increase near the slots. The analysis based on the assumption that the fluids are well mixed near the slot underestimates the drag increase while the analysis based on the assumption that the fluids do not mix near the slot overestimates the drag increase. However the estimated trend for the unmixed analysis correctly shows an increase in drag near the slot as the experimentally observed mixing decreases. More importantly it is clear that for these slots, injection flow rates, and polymer solutions, the drag increase can be explained without accounting for any swelling of the polymer solution as it leaves the slot [13,14].

Method for deducing time between bursts

The equation used to calculate the average time between bursts is based on the concept that the bursting rate per unit area is constant in a fully developed channel flow. The appropriate experimental input for this calculation is the detected number of ejections per unit time from the "full detection region" downstream of the dye slot. In this region, all of the ejections and bursts are marked by the dyed fluid. Consequently the number of ejections per unit area, f_E, is given by

$$f_E = \frac{(N_E)_{fd}}{t\,\bar{\lambda}\,\bar{n}\,\ell_d} \tag{13}$$

Here $(N_E)_{fd}$ is the number of ejections detected in the "full detection region" during the time t, while ℓ_d is the length of the "full detection region". The width over which detections are made is the product of the

average number of streaks detected, $\bar{n}$, and the average spanwise spacing of the streaks, $\bar{\lambda}$. Thus the average time between ejections detected at a point is the product of the ejection rate per unit area and the spanwise width and streamwise length over which an ejection can be detected. This latter calculations is necessary so that the Lagrangian data from the dyed fluid can be compared to the Eulerian view of an observor at a point in the flow. Using estimates from Bogard and Tiederman [10] for the area over which a burst can be detected and assuming that the previously determined average value of two ejections per burst [10,15] is valid, the equation for the average time between bursts at a point in the flow is

$$\bar{T}_B = \frac{\ell_d \, v^* \, \bar{n} \, t}{400 \, \nu \, (N_E)_{fd}} \tag{14}$$

In this study, the value of $\bar{n}$ is given by

$$\bar{n} = d_\ell / \bar{\lambda} = \frac{d_\ell \, v^*}{\lambda^+ \nu}$$

Bursting rates from 0.005-inch injection

Figure 11 shows the histograms of the number of ejections counted for the water, 16% glycerin and the 100 ppm Separan AP-273 polymer solution as a function of non-dimensional streamwise distance downstream of the 0.005-inch slot. These histograms are typical in that the number of ejections is low near the slot, increases and then decreases again farther downstream. Recall that the marked fluid must be swept into a streak and that the streaks must lift away from the wall before the streaks will burst or eject fluid. Thus some distance is required before all streaks that burst in a given region are marked. Of course when the marked fluid is depleted far downstream, the streaks bursting in that region can not be marked and detected.

The histograms for the water and 16% glycerin injection are nearly the same. The peak values in the distribution as well as the location of the distribution are very similar. Notice that the histogram for the 100 ppm solution also has the same peak values but that it is displaced downstream. This indicates that the polymer solution diffuses at a slower rate from $y^+ \leq 2$ to $y^+ = 10$ to 15 than the Newtonian fluids and yet there is no effect initially on the bursting rate at $y^+ = 15$. Since there was negligible

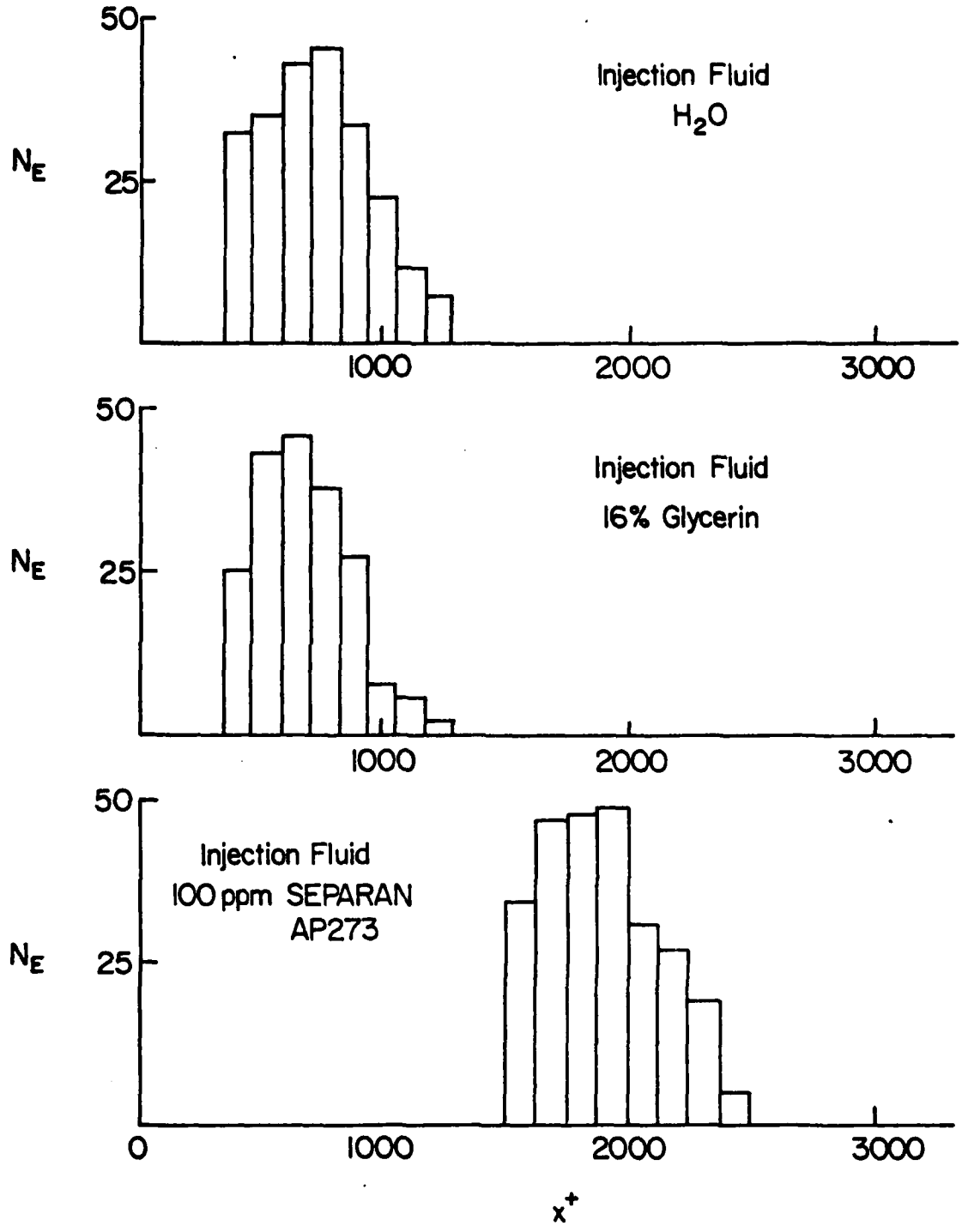

Figure 11. Histograms of detected ejections when water, 16% glycerin and 100 ppm solution of AP-273 were injected through the 0.005-inch slots, Δt=4.17 seconds.

drag reduction at $x^+ = 2000$, the fact that the bursting rate does not change at this location is consistent with the view that most of the turbulent transport occurs during bursts.

Similar results, shown in Figure 12, were found for the water, 36% glycerin and 400 ppm polymer solutions. As expected the 400 ppm solution diffused even slower into the main flow than the 100 ppm polymer solution moving the full detection region even further downstream. Results of these experiments are shown in Table 12. Again, since the peak values of the histograms are the same, the initial bursting rates are the same.

Since the full detection region for all of the fluids tested were in a region where negligible drag reduction was measured, there is no reason to suspect that the presence of the polymer would effect the streak spacing and indeed it does not [4]. Thus the approximation of $\lambda^+ = 100$ was valid for all of these experiments with the 0.005-inch slot

TABLE 12. Bursting Rate Results

Experiment number	Injection fluid	Average time between bursts (sec)	Average value of x^+ for full detection region
006	Water	0.059	725
011	16% Glycerin	0.058	650
027	AP-273 100 ppm	0.054	1800
033	36% Glycerin	0.053	850
042	AP-273 400 ppm	0.056	2500

Bursting rates from 0.050-inch inclined injection

Histograms of ejection counts as a function of distance downstream of the injector are shown in Figure 13. As before the peak values and location of the histograms for water and 16% glycerin are nearly the same. However, in this case, not only is the 100 ppm histogram shifted downstream, but the peak values are reduced significantly. When the location of the full detection region for the 100 ppm case are compared for the two different slots, it is found that the angled slot yielded a full detection region nearly 1000 wall units further downstream. Further investigation will be needed to understand this phenomenon.

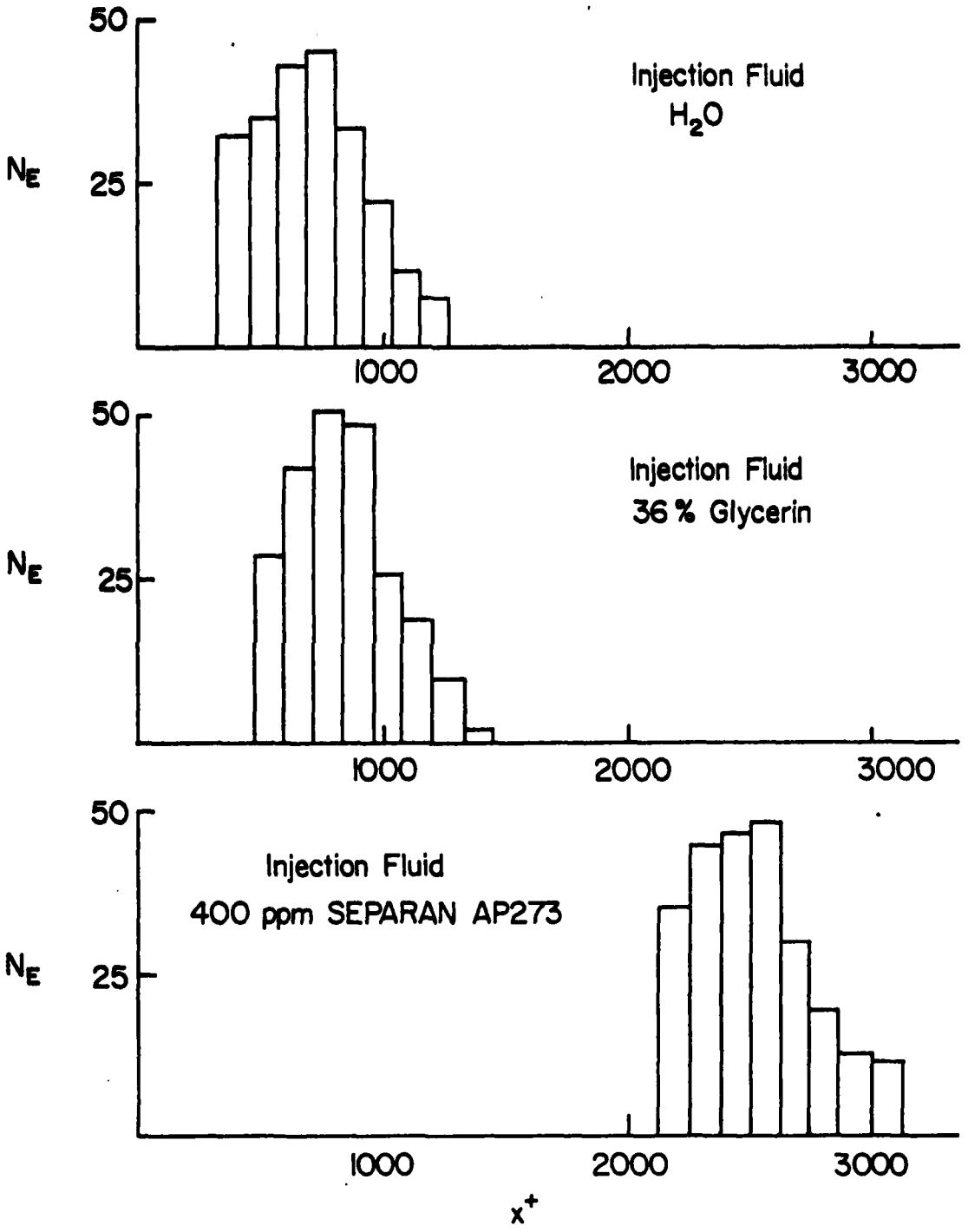

Figure 12. Histograms of detected ejections when water, 36% glycerin and 400 ppm solution of AP-273 were injected through the 0.005-inch slots, Δt=4.17 seconds.

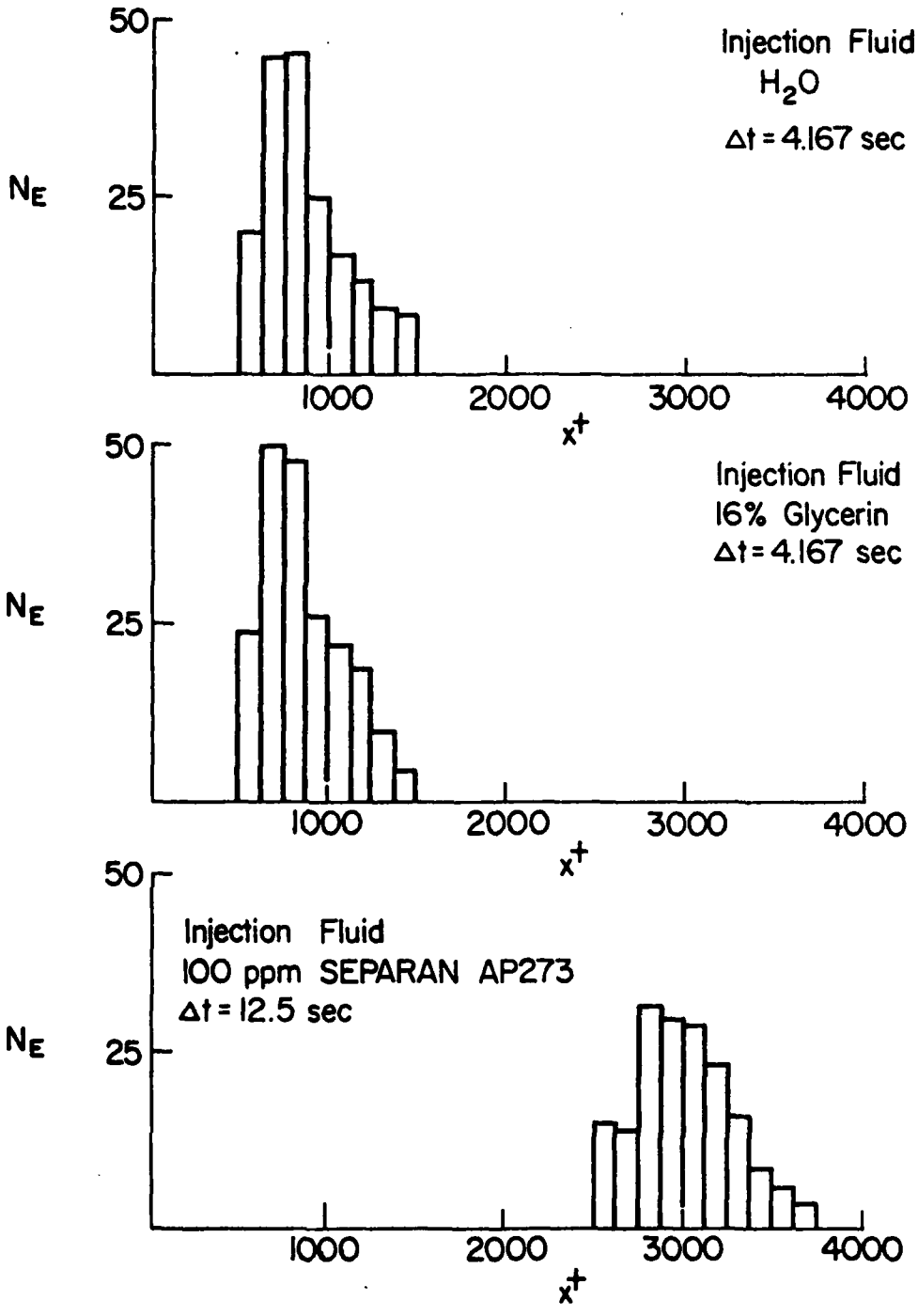

Figure 13. Histograms of detected ejections when water, 16% glycerin and 100 ppm solution of AP-273 were injected through the 0.050-inch inclined slots.

In order to calculate the average time between bursts, $\overline{T}_B$, it was necessary to determine the streak spacing for the polymer in the full detection region since an appreciable drag reduction was achieved in this region. This was done using the procedure given in the Experimental Procedures section of this report. The average streak spacing was found to be λ^+=133. As shown on Figure 14, this spacing is in good agreement with increased spacings measured in flows of homogeneous, drag-reducing solutions [11].

The resulting average time between bursts for the polymer injection is compared in Table 13 with the values for the Newtonian injections. As expected from the histograms, the average time between bursts for the drag-reducing flow has increased. Moreover it has increased more than the average spacing has increased. This aspect of the result differs from those reported earlier [7,8]. This point should be pursued because in reducing this latest data, two assumptions were made. They were that the average number of ejections per bursts and that the dimensionless area over which an ejection can be detected are the same for this drag-reducing flow as for the Newtonian cases [10].

TABLE 13. Average Bursting Rate with Drag Reduction

Experiment number	Injection fluid	Average time between bursts (sec)	Drag reduction in full detection region (percent)
111	Water	0.058	-3
124	16% Glycerin	0.053	-9
097	AP-273 100 ppm	0.143	26

Effect of Reynolds number on bursting rate

Several additional experiments were conducted to determine the effect of Reynolds number on the average time between bursts for fully developed water flows. Based on the channel width and the mass average velocity, the experiments conducted at a flow rate of 64 GPM had a Reynolds number of 17,800. Additional water experiments were conducted at Reynolds numbers of 11,000 and 15,000. Histograms of the marked ejections for each of these three Reynolds numbers are shown in Figure 15. Obviously the Reynolds number has no significant effect on the dimensionless location of the full detection

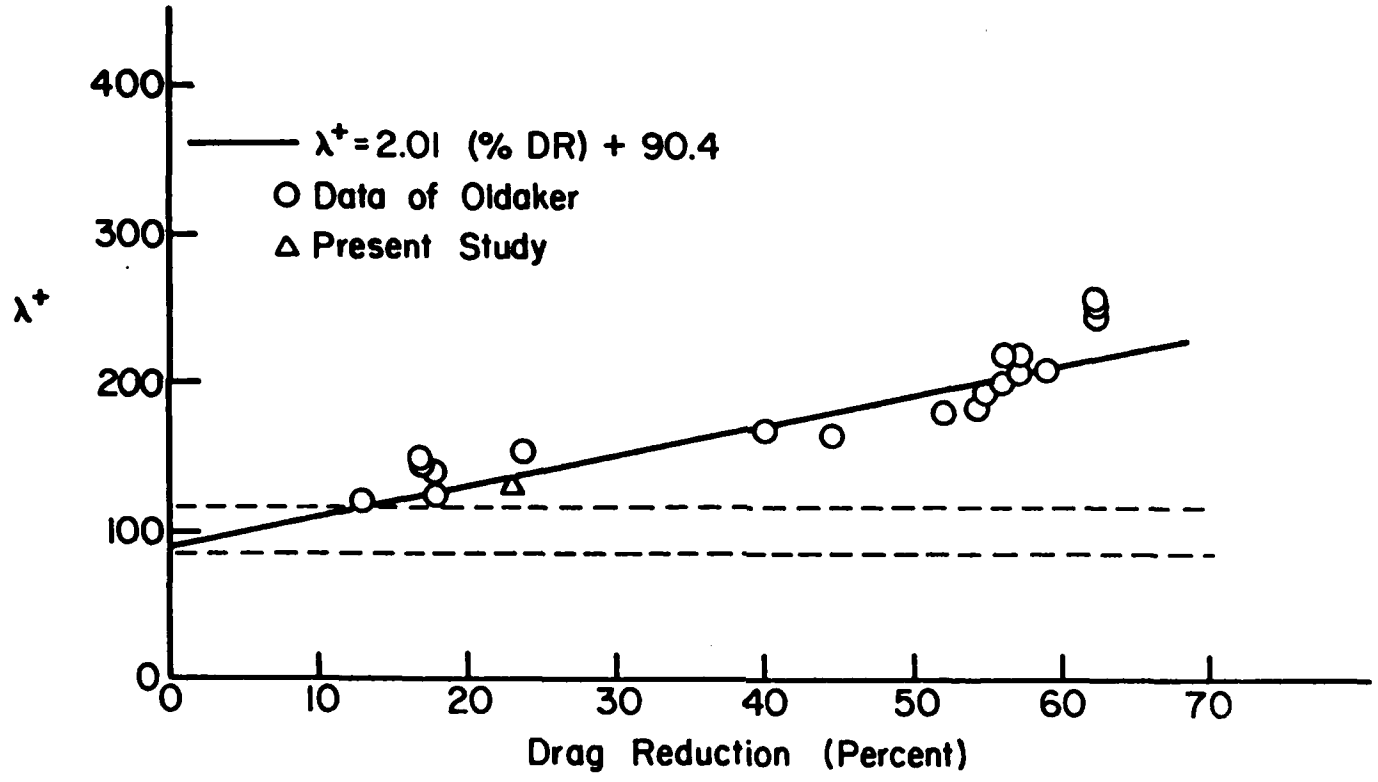

Figure 14. Effect of drag reduction on the dimensionless spanwise spacing of the sublayer streaks.

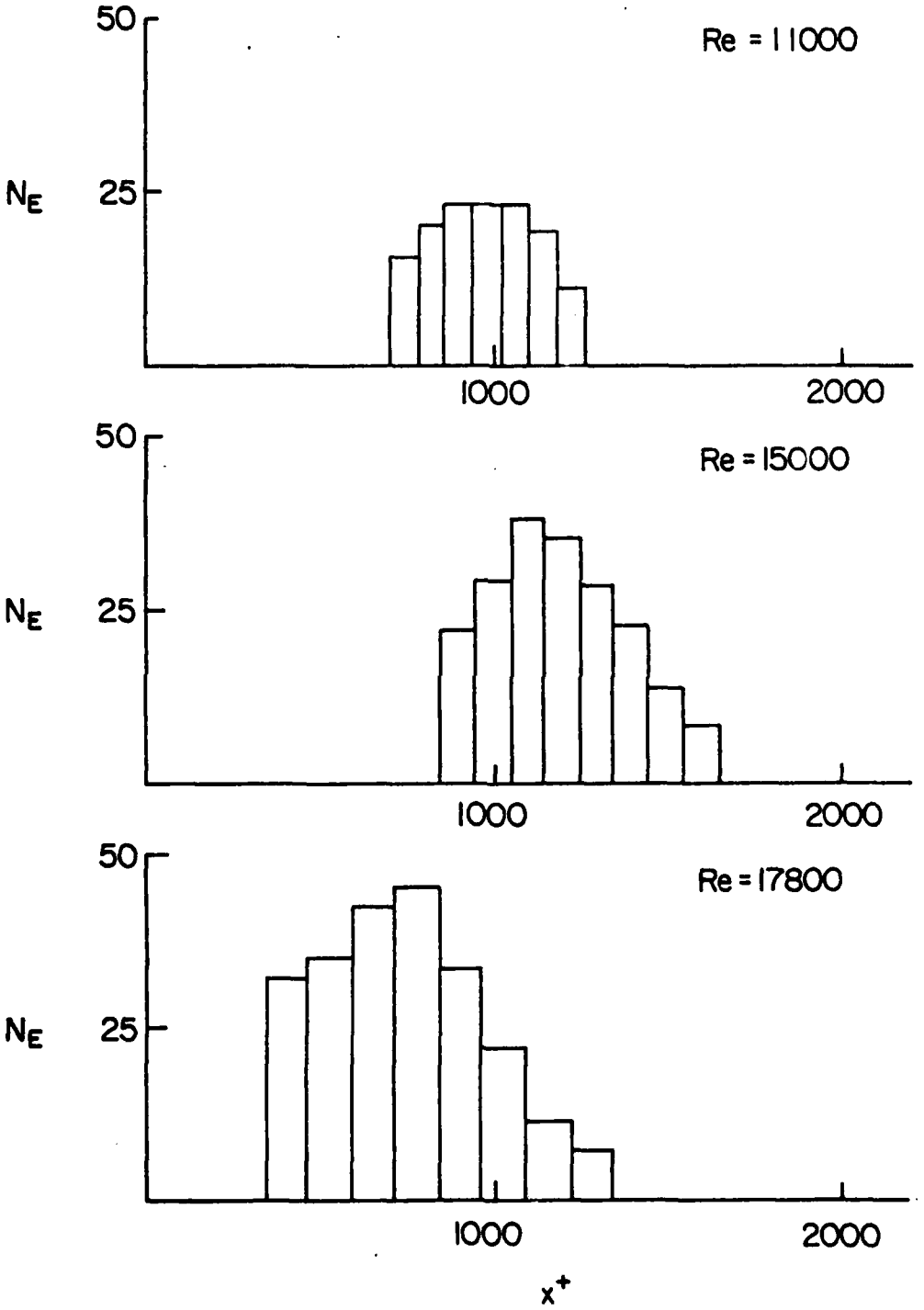

Figure 15. Histograms of ejections for fully developed water flows at various Reynolds numbers.

region. Values of $\overline{T}_B$ calculated from these histograms have been non-dimensionalized and compared to Bogard & Tiederman's [10] data at a Reynolds number of 8,700 in Figure 16 and 17.

The two common methods for normalizing $\overline{T}_B$ are to use either the inner variables of shear velocity and kinematic viscosity or the outer variables of mass average velocity and channel half-width. As shown in Figures 16 and 17, neither non-dimensionalization collapses the data to a single value. Both plots show a decrease in the dimensionless values of $\overline{T}_B$ with increasing Reynolds number. The outer variable plot, Figure 16, does a slightly better job of reducing the data to a smooth curve.

The trends shown in Figures 16 and 17 may be due to the fact that there are favorable pressure gradients in these fully developed channel flows. It has been demonstrated that favorable pressure gradients in boundary layers will increase the average time between bursts [5]. For boundary layers the appropriate dimensionless pressure gradient parameter is

$$K = -\frac{\nu}{\rho U_\infty^3}\frac{dP}{dx} \tag{16}$$

Here U_∞ is the local free-stream velocity. For two-dimensional channels this parameter becomes

$$K = -\frac{\nu}{\rho U^3}\frac{dP}{dx} \tag{17}$$

which may be rewritten as

$$K = \frac{2c_f}{Re_a}\frac{a}{D_H} \tag{18}$$

Here D_H is the hydraulic diameter of the channel. R.B. Dean [16] recommends the following correlation for the skin friction coefficient for two-dimensional channels.

$$c_f = 0.073\ Re_a^{-1/4} \tag{19}$$

When this expression is substituted into Equation 18, the following unique relationship between K and Re_a results.

$$K = 0.146\ Re_a^{-5/4}\left(\frac{a}{D_H}\right) \tag{20}$$

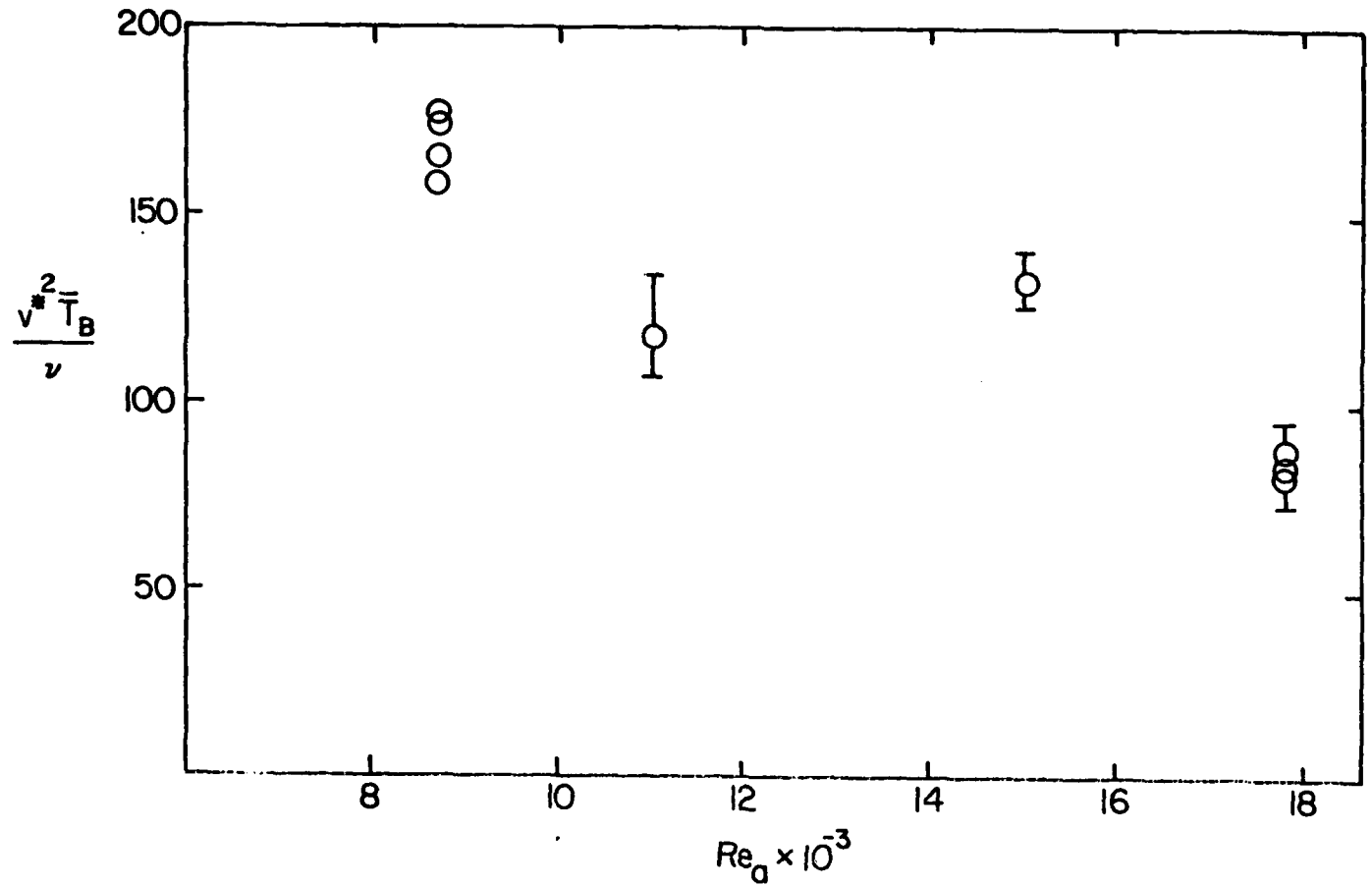

Figure 16. Effect of Reynolds number on the average time between bursts normalized with inner variables.

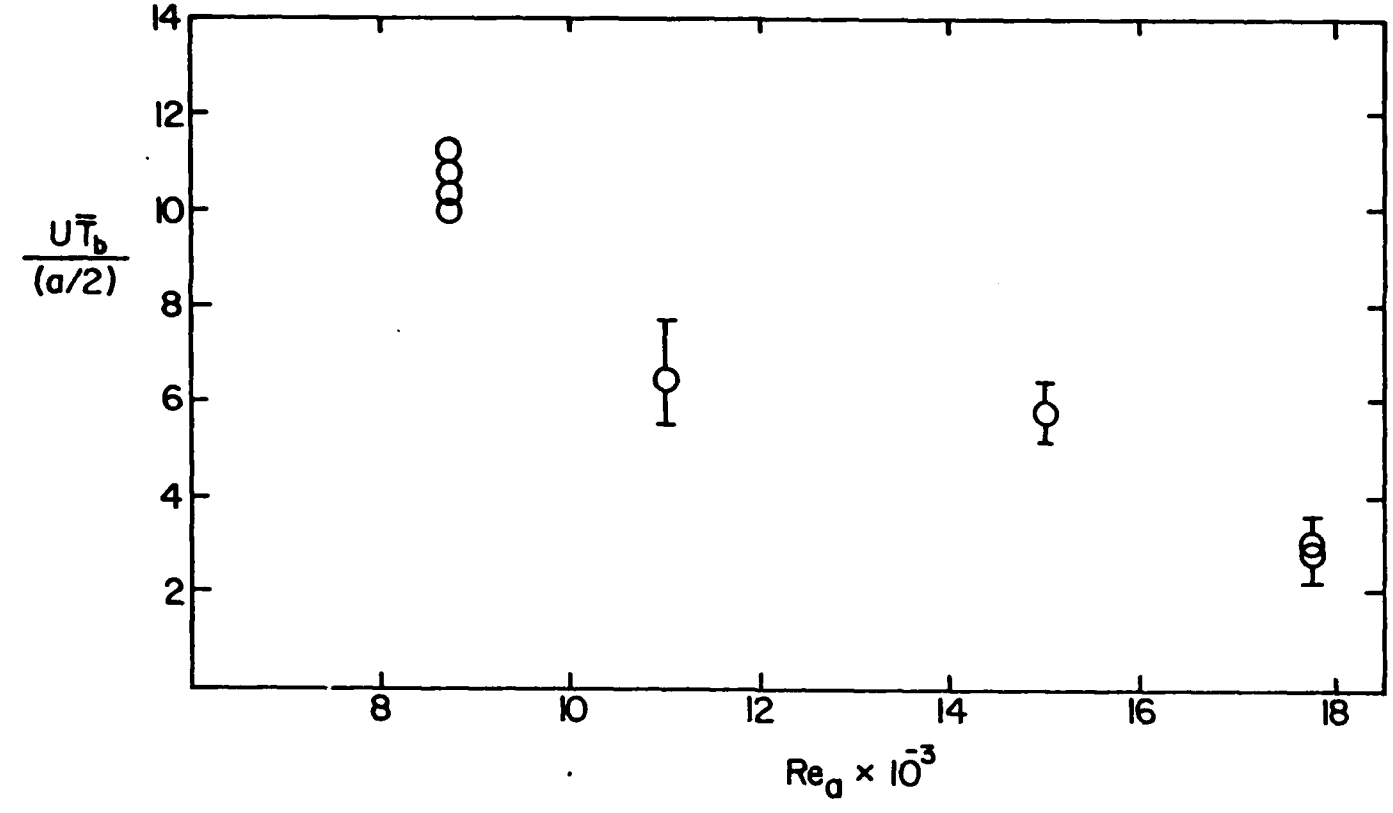

Figure 17. Effect of Reynolds number on the average time between bursts normalized with outer variables.

Thus as Re_a decreases, K increases and extrapolating the boundary layer trends, $\overline{T}_B$ should increase. Values of K for each of the points plotted in Figures 16 and 17 are given in Table 14. However also notice that the average time between bursts normalized with outer variables is lower than the commonly accepted value for zero pressure gradient boundary layers of 5±1 at a Reynolds number of 17,800.

Also shown in Table 14 are results from three experiments where the width of the light slit was varied while all other flow and visualization parameters were kept constant. These experiments verify the method used for reducing the ejection data when a light slit rather than a short dye slot is used.

TABLE 14. Bursting Rate Variation with Reynolds Number

Experiment number	Injection fluid	Reynolds number	Pressure gradient parameter $K \times 10^6$	Average time between bursts (sec)	Standard inner variables $\frac{\overline{T}_B v^{*2}}{\nu}$	Standard inner variables $\frac{\overline{T}_B U}{a/2}$
006	Water	178000	0.39	0.059	88.12	3.049
053	Water	15000	0.48	0.132	132.2	5.745
055	Water	11000	0.71	0.201	117.2	6.416
Ref. 10	Water	8700	0.96	2.300	157.8	9.890
Ref. 10	Water	8700	0.96	2.600	178.3	11.18
Ref. 10	Water	8700	0.96	2.500	171.5	10.75
Ref. 10	Water	8700	0.96	2.300	157.8	9.890
Ref. 10	Hydrogen bubbles	8700	0.96	2.400	164.6	10.32
081*	Water	17800	0.39	0.063	94.09	3.255
082**	Water	17800	0.39	0.059	88.13	3.049
083***	Water	17800	0.39	0.063	94.09	3.255
111	Water	17800	0.39	0.058	86.60	2.997

* Light plane width $d_\ell^+ = 125$

** Light plane width $d_\ell^+ = 193$

*** Light plane width $d_\ell^+ = 220$

Unless otherwise noted the light plane width is $d_\ell^+ = 188$

CONCLUSIONS AND RECOMMENDATIONS

The pressure drop and flow visualization results from the 0.005-inch slot experiments demonstrate that a thin region of drag-reducing polymer solution within only the linear, viscous sublayer does not alter the bursting rate of the wall-layer structures or lower the viscous drag. Since it has been established that the spanwise spacing of the wall-layer streaks also does not change [4], the sole modification that occurs when only the sublayer contains the drag-reducing polymer solution is a decrease in the mixing and transport between $y^+ \leq 2$ and $y^+ = 10$ to 15. These results strongly suggest that the linear sublayer is a passive participant in the interaction of the inner and outer portions of a turbulent wall layer.

Drag reduction begins downstream of the location where the injected, drag-reducing fluid has been ejected in turbulent bursts from the near-wall region. Flow visualization in the initial region of drag reduction downstream of the inclined slots shows that the dimensionless spanwise spacing of the wall-layer streaks has increased and that the average time between bursts has increased. In other words, this wall layer structure had the characteristics of the wall layer structure in a homogeneous, drag-reducing flow even through the injected polymer solution was not yet uniformly mixed with the main flow. Thus, the drag-reducing additives appear to have a direct effect on the flow structures in the buffer layer, $10 < y^+ < 100$. The upper bound cannot be established precisely from this study. However, injections studies conducted with more concentrated solutions in turbulent pipe flows [17] yielded similar bursting rate results as well as the value of $y^+ = 100$ as the upper bound of the effective region for the polymer additives.

The different drag increases near the 0.005-inch slot for the different injected fluids are consistent with the observed degree of mixing between the injected and mainstream fluids. The poor mixing of concentrated polymer solutions creates a layer of fluid near the wall that produces a blockage that accelerates the mainstream flow. Meanwhile the Newtonian fluids mix readily and produce smaller drag increases that are consistent with simply an increase in the flow rate. Different drag increases were not observed for the larger injection rates through the 0.050-inch slot. For all injeced fluids, the drag increases near the larger slot were consistent with

calculations based on the blockage model. In no case was the drag increase large enough to suggest that the polymer layer expanded or "swelled" after injection.

For the range of Reynolds numbers tested, the dimensionless average time between bursts for the water flows decreased as the Reynolds number increased. This trend is consistent with the corresponding decrease in the dimensionless pressure gradient parameter as the Reynolds number increases. However, at the largest Reynolds number the average time between bursts normalized with outer variables was less than the commonly accepted value for zero pressure gradient boundary layers. Consequently it is not yet clear how bursting rate results can be scaled to very large Reynolds numbers. Further research is needed to determine the bursting rate in both Newtonian and drag-reducing flows at large Reynolds numbers where the flow visualization techniques used in this study will not work.

While it is clear that the drag-reducing additives must be in the buffer layer, it is not clear what the optimum technique for accomplishing this is. Various combinations of polymer concentrations, injection flow rates and slot configurations need to be evaluated in a systematic way.

REFERENCES

1. Wells, C.S. and J.G. Spangler. Injection of a Drag-Reducing Fluid into Turbulent Pipe Flow of a Newtonian Fluid. The Physics of Fluids, 10, 1967, pp. 1890-1894.

2. Wu, J. and M.P. Tulin. Drag Reduction by Ejecting Additive Solutions into Pure-Water Boundary Layer. Journal of Basic Engineering, 94, 1972, pp.749-756.

3. McComb, W.D. and L.H. Rabie. Development of Local Turbulent Drag Reduction Due to Nonuniform Polymer Concentration. The Physics of Fluids, 22, 1979, pp.183-185.

4. Tiederman, W.G. and D.G. Bogard. Wall Layer Structure and Drag Reduction-Role of viscous sublayer. Report PME-FM-81-2, Purdue University, W.Lafayette, Indiana.

5. Kline, S.J., W.C. Reynolds, F.A. Schraub and P.W. Runstadler. The Structure of Turbulent Boundary Layers. J. Fluid Mech., 30, 1967, pp.741-773.

6. Kim, H.T., S.J. Kline and W.C. Reynolds. The Production of Turbulence Near a Smooth Wall in a Turbulent Boundary Layer. J.Fluid Mech., 50, 1971, pp.133-160.

7. Donohue, G.L., W.G. Tiederman and M.M. Reischman. Flow Visualization of the Near-Wall Region in a Drag-Reducing Channel Flow. J.Fluid Mech., 56, 1972, pp.559-575.

8. Achia, B.U. and D.W. Thompson. Structure of the Turbulent Boundary Layer in Drag-Reducing Pipe Flow. J.Fluid Mech., 81, 1977, pp.439-464.

9. Tiederman, W.G., A.J. Smith and D.K. Oldaker. Structure of the Viscous Sublayer in Drag-Reducing Channel Flows. Turbulence in Liquids 1975, ed. by J.L. Zakin and G.K. Patterson, Science Press, Princeton, New Jersey, 1977, pp.312-322.

10. Bogard, D.G. and W.G. Tiederman. Investigation of Flow Visualization Techniques for Detecting Turbulent Bursts. Proceedings of the Seventh Biennial Symposium on Turbulence, University of Missouri - Rolla, Rolla, Missouri, September, 1981.

11. Oldaker, D.K. and W.G. Tiederman. Spatial Structure of the Viscous Sublayer in Drag-Reducing Channel Flows. Physics of Fluids, 20, No.10, Part II, 1977, pp.S133-S144.

12. Oldaker, D.K. An Experimental Investigation of the Near-Wall Flow Structure During Drag Reduction. M.S. thesis, Oklahoma State University, Stillwater, Oklahoma, December, 1974.

13. Fruman, D.H. and P. Galivel. Near-Field Viscoelastic Effects during Thin-Slit Drag-Reducing Polymer Injection. Journal of Rheology, 24, 1980, pp.627-646.

14. Fruman, D.H. and P. Galivel. Anomalous Effects Associated with Drag-Reducing Polymer Ejection into Pure-Water Turbulent Boundary Layers. Viscous Flow Drag Reduction, Vol.72, Progress in Astronautics and Aeronautics, ed. by G.R. Hough. American Institute of Aeronautics and Astronautics, New York, NY, 1980, pp.332-350.

15. Offen, G.R. and S.J. Kline. A Comparison and Analysis of Detection Methods for the Measurement of Production in a Boundary Layer. Proceedings of the Third Biennial Symposium on Turbulence in Liquids, University of Missouri-Rolla, Rolla, Missouri, 1973, pp.289-320.

16. Dean, R.B. Reynolds Number Dependence of Skin Friction and Other Bulk Flow Variables in Two-Dimensional Rectangular Duct Flow. J.Fluids Engineering, 100, 1978, p.215.

17. McComb, W.D. and L.H. Rabie. Local Drag Reduction Due to Injection of Polymer Solutions into Turbulent Flow in a Pipe. Part I: Dependence on Local Polymer Concentration; Part II: Laser-Doppler Measurements of Turbulent Structure. AIChE Journal, 28, 1982, pp.547-565.

SYMBOLS

A_i - Surface area covered by injected fluid, $A_i = 2d\Delta x$

a - Height of channel, 0.984 inches

b - Spanwise distance over which streaks were counted

c_f - Skin friction coefficient

D - Internal diameter of tube

D_H - Hydraulic diameter

DR - Percent drag reduction

d - Spanwise length of dye slots, 8.84 inches

d_ℓ - Spanwise width of light slit

g - Acceleration of gravity

h - Manometer deflection without injection

h_i - Manometer deflection during injection

K - Dimensionless pressure gradient parameter, see Equations 16 and 17.

ℓ_d - Length of full detection region

N_E - Number of ejections

$\overline{n}$ - Average number of streaks detected

P - Static pressure

Q_i - Volumetric flow rate of injected fluid

$\overline{T}_B$ - Average time between bursts

t - Time

U - Bulk or mass average velocity

v^* - Shear velocity, $v^* = (\tau_w/\rho)^{1/2}$

w - Width of channel, 9.84 inches

x - Streamwise co-ordinate with the origin at the slots

y - Co-ordinate normal to the wall

z - Spanwise co-ordinate with origin at one side wall

Greek

Δ - Difference in the quantity that follows the symbol

δ - Blockage thickness of injected fluid

λ - Spanwise spacing of wall layer streaks

μ - Viscosity

ν - Kinematic viscosity

ρ - Density

τ_w - Wall shear stress

Superscript

$+$ - Indicates that the quantity has been made dimensionless by using the shear velocity and kinematic viscosity.

END

FILMED

6-83

DTIC